AD-A104 988 CALIFORNIA UNIV BERKELEY ELECTRONICS RESEARCH LAB F/G 20/9
PLASMA THEORY AND SIMULATION.(U)
DEC 80 C K BIRDSALL N00014-77-C-0578
UNCLASSIFIED NL

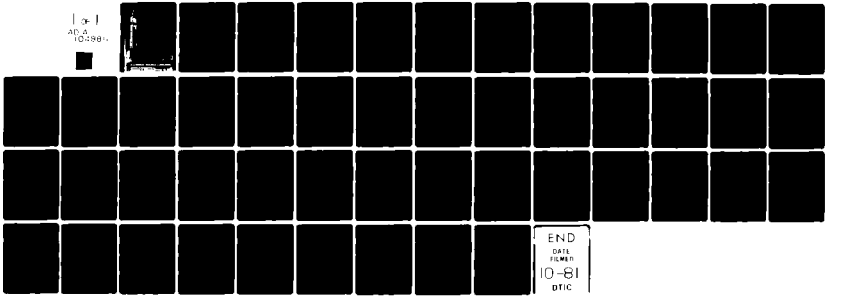

END
DATE FILMED
10-81
DTIC

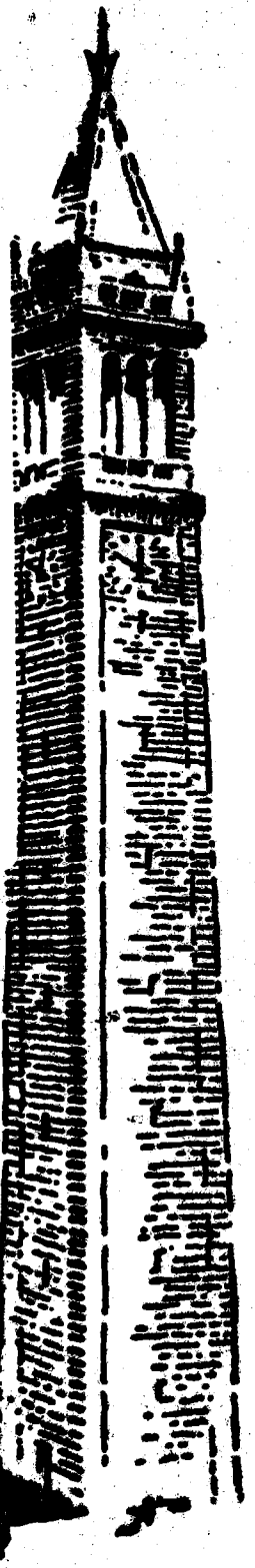

FOURTH QUARTER PROGRESS REPORT ON PLASMA THEORY AND SIMULATION

October 1, 1980 - December 31, 1980

DOE Contract AS03-76F00034-DE-AT03-76ET53064
ONR Contract N00014-77-C-0578

ELECTRONICS RESEARCH LABORATORY
College of Engineering
University of California, Berkeley, CA 94720

FOURTH QUARTER PROGRESS REPORT
on
PLASMA THEORY AND SIMULATION

October 1 to December 31, 1980

Our research group uses both theory and simulation as tools in order to increase the understanding of instabilities, heating, transport, and other phenomena in plasmas. We also work on the improvement of simulation, both theoretically and practically.

Our staff is ----

Professor C.K. Birdsall *Principal Investigator*	*191M*	*Cory Hall*	*(642-4015)*
Dr. Alex Friedman *Post Doctorate* *(Moved to LLL, Nov. 17)*	*119ME*	*Cory Hall*	*(642-3477)*
Dr. Bruce Cohen, *Dr. William Nevins* *Lecturers, UCB; Physicists LLL*	*L439* *L439*	*LLL* *LLL*	*(422-9823)* *(422-7032)*
Dr. William Fawley *Guest, UCB; Physicist LLL*	*L321*	*LLL*	*(422-9272)*
Mrs. Yu-Jiuan Chen, *Mr. Douglas Harned,* *Mr. Niels Otani,* *Mr. Stephane Rousset,* *Mr. Vincent Thomas* *Research Assistants*	*119MD*	*Cory Hall*	*(642-1297)*
Mr. H. Stephen Au-Yeung *Programmer*	*119ME*	*Cory Hall*	*(642-3477)*
Ms. Ginger Pletcher *Secretary*	*119ME*	*Cory Hall*	*(642-3477)*
Mr. Mike Hoagland *Research Typist*	*199M*	*Cory Hall*	*(642-7919)*

December 31, 1980

DOE Contract AS03-76SF00034-DE-AT03-76ET53064
ONR Contract N00014-77-C-0578

ELECTRONICS RESEARCH LABORATORY

University of California
Berkeley, California 94720

TABLE OF CONTENTS

Section I

PLASMA THEORY AND SIMULATION

Section II

CODE DEVELOPMENT AND MAINTENANCE

Section III

SUMMARY OF REPORTS, TALKS, PUBLICATIONS, VISITORS

• Indicates ONR supported areas

Section I
PLASMA THEORY AND SIMULATION

A. *Lower Hybrid Drift Instability 2d Simulations*

Yu-Jiuan Chen (Prof. C.K. Birdsall, Dr. W. Nevins, LLL)

We have improved our method of loading particles in x,y so that the initial density n(x,y) is as near our theoretical equilibrium as possible. As a result, only a small amount of electron heating was observed in the first few cycles of upper hybrid oscillations.

We have used small drift velocities ($v_E \leqslant v_{ti}$) in our simulations to date, allowing electrostatic fields, zero beta. Unfortunately, this choice makes both the growth rates and saturation levels of the lower hybrid drift instability small, hence very difficult to simulate. We are using the multibeaming quiet start loader for ion particles. Both multibeam instabilities and the lower hybrid drift instability have been observed.

A new diagnostic, gyrokinetic phase scattering plots, have been added to study the electron heating. We have been successfully subtracting the $\vec{E}\times\vec{B}$ drift corresponding to all the low frequency waves from the electron velocities. In our simulations, a small amplitude, slowly growing upper hybrid wave was observed. We found the electron gyro-kinetic energy, including electron slashing energy in the upper hybrid wave, increasing in time. However, comparing with ion temperature, electrons are still very cold.

More study of nonlinear mechanisms will be continued. Also simulations with larger drift velocities will be tried, so as to emphasize the effects sought.

B. *Magnetized Multi-Ring Instabilities*

Niels Otani, Dr. B.I. Cohen (LLL), and
Dr. M.J. Gerver (MIT) (Prof. C.K. Birdsall)

1. *Continuous rings* (M.J. Gerver)

We wish to find an approximate simple expression for the stability threshold of magnetized plasma whose distribution function consists of N monoenergetic components, arranged to approximate a Maxwellian. The dispersion relation is given by Equation (5) on p. 11 of QPR II, 1980, but with a factor of $1/N$ in front of the ion term, which was inadvertently left out of Equation (5). [The solution of Equation (5) is correct in Figure 5, p. 13 of QPR II, 1980; checked by N. Otani.] Near $\omega = l\Omega_i$ (and this is qualitatively valid as long as $|\omega - l\Omega_i| \leq \Omega_i$) we can neglect all but one term in the sum over l, and the dispersion relation becomes,

$$\frac{\omega - l\Omega_i}{l\Omega_i}\left(1 + \frac{\omega_{pe}^2}{\Omega_{e}^2}\right)\frac{\Omega_i^2}{\omega_{pi}^2} = \frac{2}{N}\sum_{s=1}^{N}\frac{\omega_{ci}}{k_\perp v_s}J_l'J_l\left(\frac{k_\perp v_s}{\Omega_i}\right)$$

$$= \frac{2}{N}\sum_{s=1}^{N}\frac{\Omega_i^2}{k_\perp^2 v_s^2}\sin\left(\frac{2k_\perp v_s}{\Omega_i}\right) \qquad (1)$$

where we have used the large argument forms of J_l and J_l' to obtain the last expression. The arguments of the sine function for two consecutive values of s differ by

$$\frac{k_\perp v_{s+1}}{\Omega_i} - \frac{k_\perp v_s}{\Omega_i} \approx \frac{k_\perp v_i}{N\Omega_i}$$

Empirically, the instability first appears at $k_\perp v_i / N\Omega_i \approx 2$, which means that the different terms in the sum over s are out of phase by ~ 2 radians, and the sum over all s is typically about equal to one of the terms in the sum.

$$\sum_{s=1}^{N} \frac{\Omega_i^2}{k_\perp^2 v_s^2} \sin\left(\frac{2k_\perp v_s}{\Omega_i}\right) \approx \frac{\Omega_i^2}{k_\perp^2 v_s^2} \approx \frac{1}{4N^2} \tag{2}$$

(Note that this result depends on regular spacing of the rings. If the values of v_s were chosen randomly, with the correct distribution function, then the sum would be greater by $\sqrt{N}$).

Instability occurs, roughly, when

$$\begin{aligned} & \omega - l\Omega_i \gtrsim \Omega_i \\ \Longrightarrow \quad & \frac{\omega - l\Omega_i}{l\Omega_i} \gtrsim \frac{1}{l} \\ \Longrightarrow \quad & \frac{\omega - l\Omega_i}{l\Omega_i} \gtrsim \frac{3}{2N} \end{aligned} \tag{3}$$

This last inequality is based on the empirical observation that instability first appears at $l \approx 2N/3$.

Combining (1) and (2) yields

$$\begin{aligned} & \frac{\omega - l\Omega_i}{l\Omega_i}\left(1 + \frac{\omega_{pe}^2}{\Omega_e^2}\right)\frac{\Omega_i^2}{\omega_{pi}^2} \approx \frac{1}{2N^3} \\ \Longrightarrow \quad & \frac{\omega - l\Omega_i}{l\Omega_i} \approx \frac{\omega_{pi}^2}{\Omega_i^2}\left(1 + \frac{\omega_{pe}^2}{\Omega_e^2}\right)^{-1}\frac{1}{2N^3} \end{aligned} \tag{4}$$

Combining (3) and (4) gives the condition for stability:

$$N^2 \gtrsim \frac{1}{3}\frac{\dfrac{\omega_{pi}^2}{\Omega_i^2}}{1 + \dfrac{\omega_{pe}^2}{\Omega_e^2}} \tag{5}$$

This result differs by N from the rule given in QPR III, p. 2, 1980; some reconciliation is needed. In practice, we must use an "effective N", which is the number of terms in the sum over s which contribute significantly to the sum. This number will be quite a bit less (maybe by a factor of 6) than the total number of terms N. In principle, however, ω_{pi}^2/Ω_i^2 should go as N^2 for sufficiently large N. For N sufficiently large [probably something like $3(m_i/m_e)^{1/2}$ in practice], there will be no instability.

2. *An Electrostatic Dispersion Relation for a Uniform Magnetized Plasma Having a Discrete-Particle or Rings-and-Spokes Velocity Distribution* (Niels F. Otani and Bruce I. Cohen)

We continue to examine the electrostatic instability associated with particle velocity distributions found in plasma simulation computer codes. In the previous QPR the analysis of this instability was based on the behavior of the equilibrium distribution $f_0 = \sum_n a_n \delta(v_\perp - v_{\perp n})$. We now extend the analysis to include the discreteness of particles in gyrophase space ("rings and spokes"). As before, the equilibrium is assumed to be spatially uniform and uniformly magnetized.

The derivation in (a) is due to Otani. Cohen offers an alternative derivation in (b) based on action-angle variables that confirms the analysis in (a) but is simpler and more compact. Conclusions are presented in (c).

(a) Derivation of the Dispersion Relation

We choose as our phase-space coordinates μ, θ', X, Y, z, and v_z where, in terms of the usual cartesian phase-space coordinates,

$$\mu = \frac{v_x^2 + v_y^2}{2\Omega} \tag{1}$$

$$\theta' = \arctan \frac{v_x}{v_y} - \Omega t \tag{2}$$

$$X = x + \frac{v_y}{\Omega} \tag{3}$$

$$Y = y - \frac{v_x}{\Omega} \tag{4}$$

Here $\Omega = \frac{eB_0}{mc}$. Note the explicit time dependence of θ' on t.

We wish to consider equilibria of the form

$$f_0 = f_0(\mu, v_z, \theta') \tag{5}$$

These are valid equilibria since μ, v_z, and θ' are all constants of the motion. In particular, θ' is the gyrophase measured relative to a corotating reference angle and hence is constant along an equilibrium trajectory.

The linear dispersion relation is obtained by considering the perturbed distribution

$$f = f_0(\mu, v_z, \theta') + \delta f(\mu, v_z, \theta', X, Y, t) \tag{6}$$

Notice in this derivation we are only considering modes with spatial dependence in the plane perpendicular to the magnetic field $B_0\hat{z}$. Also it is assumed these modes are collisionless:

$$\frac{df}{dt} = 0 \tag{7}$$

This equation combined with the equations of motion

$$\dot{\mathbf{v}} = \frac{e}{m}\delta\mathbf{E} + \frac{e}{mc}\mathbf{v}\times\mathbf{B}_0 \tag{8}$$

yields the linearized equation

$$\frac{\partial \delta f}{\partial t} + \frac{e}{m\Omega}\mathbf{v}_\perp\cdot\delta\mathbf{E}_\perp + \frac{e}{m\Omega}\delta\mathbf{E}\times\mathbf{v}_\perp\cdot\hat{\mathbf{z}}\frac{1}{2\mu}\frac{\partial f_0}{\partial \theta'} = 0 \tag{9}$$

Here the assumptions $\delta\mathbf{E} = -\nabla\phi$ (electrostatic assumption) and $\partial/\partial z = 0$ have been used. Fourier transforming the time dependence we have:

$$i\omega\delta f(\mathbf{z},\omega) = \frac{e}{m\Omega}\left[\frac{\partial f_0}{\partial \mu}\int dt\; e^{i\omega t}\mathbf{v}_\perp\cdot\delta\mathbf{E}_\perp + \frac{1}{2\mu}\frac{\partial f_0}{\partial \theta'}\int dt\; e^{i\omega t}\delta\mathbf{E}_\perp\times\mathbf{v}_\perp\cdot\hat{\mathbf{z}}\right] \tag{10}$$

in which, for brevity, $\mathbf{z} = (\mu, v_z, \theta', X, Y)$. It is interesting to note that the explicit time dependence of $\mathbf{v}_\perp(\mathbf{z},t)$ leads to the coupling of different frequency components:

$$\delta f(\mathbf{z},\omega) = \frac{er_g}{2m\omega}\left[e^{i\theta'}\delta E^+(\mathbf{z},\omega+\Omega)\left(\frac{\partial f_0}{\partial \mu} + \frac{i}{2\mu}\frac{\partial f_0}{\partial \theta'}\right)\right. \tag{11}$$

$$\left. - e^{-i\theta'}\delta E^-(\mathbf{z},\omega-\Omega)\left(\frac{\partial f_0}{\partial \mu} - \frac{i}{2\mu}\frac{\partial f_0}{\partial \theta'}\right)\right] \tag{12}$$

Here $r_g \equiv v_\perp/\Omega$ and $\delta E^\pm = \delta E_x \pm i\delta E_y$. Another equation for $\delta\mathbf{E}$ is obtained as follows

$$\delta\mathbf{E}(\mathbf{z},\omega) = -\int dt\; e^{i\omega t}(\nabla\phi)(\mathbf{z},t) \tag{13}$$

where

$$(\nabla\phi)(\mathbf{z},t) = \nabla\phi(x,y,t)\Big|_{\substack{x = X + r_g\cos(\theta'+\Omega t)\\ y = Y - r_g\sin(\theta'+\Omega t)}} \tag{14}$$

Defining $\mathbf{x}_\perp = (x,y)$, $\mathbf{k}_\perp' = (k_x',k_y')$, and $\mathbf{X} = (X,Y)$, we have

$$\nabla\phi(\mathbf{x}_\perp,t) = \int \frac{d^2k_\perp'}{(2\pi)^2}\int \frac{d\omega'}{2\pi}\; e^{i(\mathbf{k}_\perp'\cdot\mathbf{x}_\perp - \omega' t)} i\mathbf{k}_\perp'\phi(\mathbf{k}_\perp',\omega') \tag{15}$$

Now substituting back into Eq. (14):

$$\phi(\mathbf{z},t) = \int \frac{d^2k_\perp'}{(2\pi)^2}\; e^{i\mathbf{k}_\perp'\cdot\mathbf{X}} e^{ik_\perp' r_g \sin(\theta'+\Omega t-\alpha')} e^{-i\omega' t}\phi(\mathbf{k}_\perp',\omega') \tag{16}$$

where $k_x' = -|\mathbf{k}_\perp'|\sin\alpha'$ and $k_y' = -|\mathbf{k}_\perp'|\cos\alpha'$. With the help of the usual Bessel identity, we obtain

$$\delta\mathbf{E}(\mathbf{z},\omega) = -\int \frac{d^2k_\perp'}{(2\pi)^2}\; e^{i\mathbf{k}_\perp'\cdot\mathbf{X}}\sum_{l'} J_{l'}(k_\perp' r_g) e^{il'(\theta'-\alpha')} i\mathbf{k}_\perp'\phi(\mathbf{k}_\perp',\omega+l'\Omega) \tag{17}$$

A third equation may be found from

$$\rho(\mathbf{x},t) = \int d\mathbf{z}\; en_0\delta^3(\mathbf{x} - \mathbf{r}(\mathbf{z},t))\delta f(\mathbf{z},t) \tag{18}$$

where n_0 is the unperturbed number density, ρ is the perturbed charge density, and $\mathbf{r}(\mathbf{z},t)$ are the spatial cartesian coordinates as functions of $\mathbf{z}$ and t. Fourier transforming,

$$\rho(\mathbf{k},\omega) = en_0\int dt\; e^{i\omega t}\int d\mathbf{z}\; e^{-i\mathbf{k}\cdot\mathbf{r}(\mathbf{z},t)} \tag{19}$$

Using Poisson's equation and the Bessel identity again,

$$\phi(\mathbf{k},\omega) = \frac{4\pi en_0}{k^2}\int d\mathbf{z}\; e^{-ik_z z} e^{-i\mathbf{k}_\perp\cdot\mathbf{X}}\sum_l J_l(k_\perp r_g) e^{-il(\theta'-\alpha)}\delta f(\mathbf{z},\omega - l\Omega) \tag{20}$$

where $k_x = -|\mathbf{k}_\perp|\sin\alpha$ and $k_y = -|\mathbf{k}_\perp|\cos\alpha$. Substituting (12) and (17) into (20) we obtain

$$\phi(\mathbf{k}_\perp,\omega) = -\frac{\omega_p^2}{k_\perp^2}\int d\mu\; d\theta' \sum_l\sum_{l'} \frac{J_l(k_\perp r_g)J_{l'}(k_\perp r_g)}{\omega - l\Omega} \tag{21}$$

$$\times\left[\frac{e^{i(l'-l+1)(\theta'-\alpha)}}{2}\left(\frac{\partial g_0}{\partial\mu} + \frac{i}{2\mu}\frac{\partial g_0}{\partial\theta'}\right)\phi(\mathbf{k}_\perp,\omega+(l'-l+1)\Omega\right) \tag{22}$$

$$+\frac{e^{i(l'-l-1)(\theta'-\alpha)}}{2}\left(\frac{\partial g_0}{\partial\mu} - \frac{i}{2\mu}\frac{\partial g_0}{\partial\theta'}\right)\phi(\mathbf{k}_\perp,\omega+(l'-l-1)\Omega)\Bigg] \tag{23}$$

where $\omega_p \equiv (4\pi n_0 e^2/m)^{1/2}$ and $g_0 \equiv \int dv_z\; f_0$.

The determinant of the implied (infinite) matrix serves as the dispersion function for the general case $f_0 = f_0(\mu, v_z, \theta')$. Equation (23) assumes only one contributing species of particles; generalization to more species is straightforward. Notice that the eigenmodes for this system do not in general have the simple time dependence $e^{-i\omega t}$, but instead are composed of a mixture of frequencies Ω apart. This is a consequence of the time-dependent equilibrium f_0. As a check we find that the well-known gyrophase-independent dispersion relation

$$1 + \frac{\omega_p^2}{k_\perp^2}\int 2\pi\; d\mu\; \frac{\partial g_0}{\partial\mu}\sum_l \frac{lJ_l^2(k_\perp r_g)}{\omega - l\Omega} = 0 \tag{24}$$

is recovered when $\partial g_0/\partial\theta' = 0$. Also Eq. (23) is found to be consistent with the reality

condition $\phi^*(\mathbf{k}_\perp,\omega) = \phi(-\mathbf{k}_\perp,-\omega)$.

Now choose $g_0(\mu,\theta')$ to be the discrete-particle velocity distribution

$$g_0(\mu,\theta') = \sum_n a_n \delta(\mu - \mu_n) \sum_{m=1}^{M_n} \delta(\theta' - (\frac{2\pi m}{M_n} + \theta_n)) \tag{25}$$

where a_n, θ_n, μ_n, and M_n are constants. In this case Eq. (23) reduces to

$$\phi(\mathbf{k}_\perp,\omega) = \frac{\omega_p^2}{k_\perp^2} \sum_{l,n,j} a_n M_n \frac{e^{ijM_n(\theta_n-\alpha)}}{2} \frac{k_\perp r_n}{\mu_n} \tag{26}$$

$$\times \frac{(l+jM_n)J_l' J_{l+jM_n} + lJ_l J'_{l+jM_n}}{\omega - l\Omega} \phi(\mathbf{k}_\perp,\omega - jM_n\Omega) \tag{27}$$

The argument of all Bessel functions is $k_\perp r_n$; r_n is the gyroradius corresponding to μ_n.

For the rings-and-spokes distribution, $M_n \equiv M$ and $\theta_n \equiv \Theta$ for all n. Equation (27) may now be written as

$$\phi(\mathbf{k}_\perp,\omega+jM) = \sum_{j'} A_{j,j'} \phi(\mathbf{k}_\perp,\omega+j'M) \tag{28}$$

where

$$A_{j,j+\Delta j} = \frac{\omega_p^2}{\Omega^2} \sum_l \frac{D(l+jM,\Delta j)}{\frac{\omega}{\Omega} - l} \tag{29}$$

and

$$D(l,\Delta j) = \sum_n \frac{a_n}{k_\perp r_n} e^{iM\Delta j(\Theta-\alpha)} [lJ_l J'_{l+M\Delta j} + (l+M\Delta j) J_{l+M\Delta j} J_l'] \tag{30}$$

We find that A is hermitian when ω is real and see that only terms such that $M|\delta j| \leqslant 2k_\perp(r_n)_{\max}$ contribute since $J_l(k_\perp r_n)$ goes to zero very rapidly once $|l|$ is appreciably larger than $k_\perp r_n$. In particular, if $M \geqslant 2k_\perp(r_n)_{\max}$ only diagonal terms contribute. In other words, the rings-and-spokes distribution behaves essentially like the corresponding gyrophase-independent distribution when the wavelength is longer than the spacing of M particles arranged on a circle of radius $(r_n)_{\max}$.

(b) Alternative Derivation

An alternative and somewhat simpler derivation is based on the use of action-angle variables as described in *Aamodt et al.* (1981). The Vlasov equation can be written as

$$f(t) - f(0) = \int_{-\infty}^{t} dt' \{H,f\}, \tag{31}$$

where H is the Hamiltonian and { } is the Poisson bracket. The single particle Hamiltonian for a flute mode ($\mathbf{k}\cdot\mathbf{B} = 0$) is

$$H = H_0 + H_1 = \mu\Omega + q\tilde{\phi} \exp(ikx - i\omega t) + c.c. = \tag{32}$$

$$\mu\Omega + q\tilde{\phi} \sum_n J_n(kv_\perp/\Omega) \exp(in\theta - i\omega t) + c.c., \tag{33}$$

where X and Y are the x and y guiding center positions, $\mu \equiv mv_\perp^2/2\Omega$, $\theta = \arctan v_x/v_y$, $\Omega \equiv qB_0/mc$, B_0 is a uniform external magnetic field in the z direction, and $\mathbf{k}$ has been taken parallel to $\hat{\mathbf{x}}$ without loss of generality. The Vlasov equation can be linearized with respect to H_1/H_0:

$$f_1 = \int_{-\infty}^{t} dt' \left(\frac{\partial H_1}{\partial\theta} \frac{\partial f_0}{\partial\mu} - \frac{\partial H_1}{\partial\mu} \frac{\partial f_0}{\partial\theta} \right) \tag{34}$$

In Eq. (34), the equilibrium distribution function f_0 has been taken to be independent of X and Y, as we assume the plasma to be uniform.

Canonical transformation to the new variables $(\bar{\theta},\bar{\mu})$ using the generating function $F_2 = (\theta - \Omega t)\bar{\mu}$ gives $\bar{\theta} = \partial F_2/\partial\bar{\mu} = \theta - \Omega t$, $\mu = \bar{\mu} = \partial F_2/\partial\theta$, and $\bar{H} = H + \partial F_2/\partial t = e\phi$, where

$$e\phi = e\tilde{\phi}\sum_n J_n \exp\ [in(\bar{\theta}+\Omega t) - i\omega t] + c.c. \tag{35}$$

To zero order in the perturbation $e\phi$, the equations of motion are trivial,

$$\frac{d}{dt}(\bar{\theta},\bar{\mu};X,Y)^{(0)} = 0; \tag{36}$$

all of the independent variables are now constants of the zero order motion. A suitable equilibrium distribution function composed of N_θ angular spokes is given by

$$f_0 = n_0 N_\theta^{-1} \sum_{j=1}^{N_\theta} \delta(\bar{\theta} - \theta_j) f_0(bar). \tag{37}$$

Equation (34) becomes

$$f_1 \exp\ (ikx - i\omega t) = -q\tilde{\phi} \sum_n \frac{nJ_n\dfrac{\partial f_0}{\partial\bar{\mu}} + i\dfrac{\partial J_n}{\partial\bar{\mu}}\dfrac{\partial f_0}{\partial\bar{\theta}}}{\omega - n\Omega}\exp\,[in(\bar{\theta}+\Omega t) - i\omega t]. \tag{38}$$

Use of Poisson's equation $-\nabla^2\phi = 4\pi\sum_s q_s\int d^3v\ f_{1s}$ enables us to obtain a dispersion relation

$$k^2\tilde{\phi} = 4\pi\sum_s q_s \int d\bar{\mu}d\bar{\theta}\ f_{1s} = \tag{39}$$

$$4\pi\sum_s n_0 q^2\int d\bar{\mu} f_0(\bar{\mu})\sum_{l,n}\frac{n\dfrac{\partial}{\partial\bar{\mu}}(J_l J_n) - (n-l)J_l\dfrac{\partial J_n}{\partial\bar{\mu}}}{\omega - n\Omega} \tag{40}$$

$$\times\ N_\theta^{-1}\sum_j \exp\ [i(n-l)(\theta_j+\Omega t)]\tilde{\phi} \tag{41}$$

If the angles θ_j are evenly spaced, $\theta_j = (j-1)2\pi/N_\theta$, then

$$N_\theta^{-1}\sum_j \exp\ [i(n-l)(\theta_j+\Omega t)] = \exp\,[i(n-l)\Omega t]\delta_{n,l+N_\theta m}, \tag{42}$$

where δ_{ij} is the Kronecker delta and $m = 0,\pm1,\cdots$. Hence,

$$k^2\tilde{\phi} = k^2\sum_r\tilde{\phi}_r \exp\ (ir\Omega t) = \sum_s 4\pi n_0 q^2\int d\bar{\mu}\ f_0(\bar{\mu})\sum_p\tilde{\phi}_p \tag{43}$$

$$\times\sum_{l,n}\frac{n\dfrac{\partial}{\partial\bar{\mu}}(J_l J_n) - (n-l)J_l\dfrac{\partial J_n}{\partial\bar{\mu}}}{\omega - p\Omega - n\Omega}\delta_{n,l+mN_\theta}\exp\ [i(n-l+p)\Omega t], \tag{44}$$

from which follows

$$\tilde{\phi}_r = \sum_s\frac{4\pi n_0 q^2}{k^2}\int d\bar{\mu} f_0(\bar{\mu})\left\{\tilde{\phi}_r\sum_n\frac{n\dfrac{\partial}{\partial\bar{\mu}}(J_n^2)}{(\omega-r\Omega)-n\Omega}\right. \tag{45}$$

$$\left. + \sum_{\substack{n,m\\ m\neq0}}\tilde{\phi}_{r-mN_\theta}\frac{n\dfrac{\partial}{\partial\bar{\mu}}(J_n J_{n-mN_\theta}) - mN_\theta J_{n-mN_\theta}\dfrac{\partial J_n}{\partial\bar{\mu}}}{\omega - r\Omega - n\Omega + mN_\theta\Omega}\right\} \tag{46}$$

Equation (28) in (a) is easily recovered from this expression.

The discrete evenly spaced angles have produced an alias coupling of temporal modes separated in frequency by $mN_\theta\Omega$, where $m = 0, \pm 1, \pm 2, \cdots$ As argued in (a), we can arrange for the coupling to be weak and thus recover the desired dispersion relation for an equilibrium with no gyrophase structure,

$$1 = \frac{4\pi}{k^2} \sum_s n_0 q^2 \int d\bar{\mu}\, f_0(\bar{\mu}) \sum_n \frac{n \frac{\partial}{\partial \bar{\mu}} (J_n^2)}{\omega - n\Omega}, \tag{47}$$

if the coefficients multiplying $\bar{\phi}_{r-mN_\theta}$ for $m \neq 0$ are negligible, so that only the coupling of $\bar{\phi}_r$ to itself survives in Eq. (46). For small argument, the Bessel function has the limiting form $J_\nu(z) \sim (z/2)^\nu/\nu!$, and $|J_\nu(z)| << 1$ for $|z| < \nu/2$. In a typical simulation with a thermal velocity distribution, $\max(v_\perp) < 4v_{th}$. Hence the argument of the Bessel functions in Eq. (46) satifies the inequality $z = kv_\perp/\Omega < (4k_{\max}v_{th}/\Omega)$. The coupling of $\bar{\phi}_r$ to $\bar{\phi}_{r-mN_\theta}$ will be negligible if

$$N_\theta > (8k_{\max}v_{th}/\Omega). \tag{48}$$

The analysis of Kim and Otani in QPR II, 1980 describing the multi-beaming instability of a warm magnetized plasma made up of many rings forming a Maxwellian velocity distribution can then be applied to Eq. (47). Generally speaking, for $N_{v_\perp}$ equally weighted rings, stability can be achieved for

$$N_{v_\perp} > \frac{1}{3}\left(\frac{\omega_p}{\omega_c}\right)^2. \tag{49}$$

Thus, a quiet-start simulation ought to be *stable* to magnetized multi-ring instabilities if the inequalities in Eqs. (48) and (49) are both satisfied.

(c) Conclusions

In conclusion, dispersion functions for the general distribution $f_0(\mu, v_z, \theta')$, the discrete-particle distribution, and the rings-and-spokes distribution have been derived and found to be consistent with well-known gyrophase-independent dispersion relations. We find that the eigenmodes are in general not simple sinusoidal functions of time but are instead a mixture of frequencies. However, in the case of the rings-and-spokes distribution it was shown that the different frequencies decouple when the number of particles per ring (i.e., number of spokes) becomes somewhat larger than $k_\perp(r_n)_{\max}$ in which case the dispersion relation reduces to its gyrophase-independent counterpart. With a sufficient number of discrete θ' and μ classes (spokes and rings) it should then be possible to perform quiet-start simulations that are stable to magnetized multi-ring instability.

(d) Acknowledgments

We are grateful to W. M. Nevins for a number of illuminating discussions and to C. K. Birdsall for his interest and encouragement. The research of B. I. Cohen was performed under the auspices of the U. S. Department of Energy at Lawrence Livermore National Laboratory under Contract W-7405-ENG-48. *Reference*

R. E. Aamodt, B. I. Cohen, Y. C. Lee, C. S. Liu, D. R. Nicholson, and M. N. Rosenbluth, *Phys. Fluids*, **24**, 55, (1981).

C. *Long Field-Reversing Ion Layers*

Douglas S. Harned (Prof. C.K. Birdsall)

(1) Paper

The paper following (3) was presented at the Third Symposium on the Physics and Technology of Compact Toroids in the Magnetic Fusion Energy Program held at Los Alamos, New Mexico, Dec. 2-4, 1980. It summarizes work on ion layer kink instabilities done through the end of October 1980.

(2) Code Development

The following modifications have been made during November and December to our two-dimensional hybrid code, AQUARIUS: (a) The mover has been vectorized, producing a factor of 2.7 increase in efficiency. (b) Finite electron pressure has been included. (c) A new version has been developed which employs conducting wall boundaries and has the capability to handle vacuum regions.

(3) Results

Two new results have been obtained from AQUARIUS: (a) New diagnostics have enabled measurement of the real part of the frequencies of ion layer kink instabilities. These frequencies have been found to agree with theoretical predictions. (b) Saturation of ion layer kink instabilities has been found to be due to heating of the layer. The heating, which occurs during instability growth, causes the layer to thicken. As the layer becomes thicker the betatron frequency of the layer particles is reduced. Once the betatron frequency has become sufficiently low, then the self-magnetic field index drops below the instability threshold value and the instability ceases to grow.

Kink Motion of Long Field-Reversing Ion Layers

Douglas S. Harned

Electronics Research Laboratory
University of California
Berkeley, California 94720

Kink instabilities have been studied in long field-reversing ion layers. The configuration is shown in Figure. 1. An ion beam, at radius R and of thickness a, crosses an external magnetic field $B_e = B_z^e \hat{z}$. The beam current, $J_{b\theta}^s$, produces a self-magnetic field, B_z^s, which tends to reverse the total magnetic field on axis. The layer is immersed in a uniform background plasma such that $n_b << n_p$, where n_b and n_p are the densities of the beam and plasma, respectively. There is assumed to be no variation in the axial direction (i.e., $\partial/\partial z = 0$). Kink modes in these layers correspond to perturbations of the form $\epsilon = \epsilon_r \exp(in\theta - i\omega t)\hat{r}$, with $n \geq 2$.

Long layer kink modes have been studied by Lovelace[1]. Analytic results were obtained for uniform layers with sharp boundaries within the approximations $(a/R)^2 << 1$, $(\omega/n\Omega)^2 << 1$, and $v_A^2 \approx$ constant, where Ω is the layer rotation frequency and v_A the plasma Alfven velocity. Stability thresholds were obtained for two cases: (1) $\omega^2 << (v_A/a)^2$ and (2) $\omega^2 < (v_A/a)^2$ with $\omega_r^2 << \omega_i^2$, where ω_r and ω_i are the real and imaginary parts of the frequency. In both cases the condition $\eta_s < n^2 - 1$ was found to be sufficient for stability, where η_s is the self-magnetic field index. If ζ is defined to be the loading factor $(\zeta \equiv |B_z^s(r=0)/B_z^e|)$, then η_s is of order $(2R/a)\zeta$.

In order to have a useful comparison for our simulation results it was necessary to generalize the preceding theoretical analysis by eliminating the assumptions $\omega^2 < (v_A/a)^2$, $\omega_r^2 < \omega_i^2$, and $v_A^2 \approx$ constant. In addition we chose to study the stability of a rigid rotor distribution. The approximations were eliminated by performing a numerical solution of Lovelace's equations. With the less severe constraints on frequencies our numerical results produced more restrictive requirements on the self-magnetic field index for stability. Minimum values of η_s for

instability are shown in Table 1. It can be seen that the thresholds increase with increasing background density.

A two-dimensional simulation code, AQUARIUS, has been developed and applied to ion layer kink motion. The code treats ions as particles and electrons as a massless fluid. The Darwin version of Maxwell's equations are used (i.e. the transverse displacement current is neglected). Maxwell's equations are coupled with the electron momentum equation (with inertial terms neglected) by the assumption of quasineutrality to determine the time evolution of the electric and magnetic fields. The ion particles obey the equations of motion. Standard particle-in-cell techniques are employed to determine forces and accumulate currents.

The code is initialized with an equilibrium exponential rigid rotor ion layer distribution. Instabilities have been observed corresponding to n=2,3,4, and 5 modes. Figure 2 shows the particle positions in their initial state for a layer with $\zeta \simeq 1.4$. In Fig. 3 the particle positions of this same layer have become significantly perturbed after an n=3 mode has grown to large amplitude. When linear growth rates from simulations are compared with the predictions of our numerical extension of the theory in Ref. 1, excellent agreement is obtained. The simulation results and the corresponding theoretical growth rates for an ion layer with $R/a \simeq 5$ are shown in Figs. 4 and 5. The maximum growth rate for a given mode occurs at $n \simeq \omega_\beta/\Omega$, where ω_β is the layer betatron frequency. Figure 5 shows how the growth decreases with increasing background plasma density. Nonlinear effects have been found to halt the linear growth of kink instabilities. The saturation amplitudes decrease with increasing azimutha' mode number. The instabilities have been observed to grow and saturate without destroying the field-reversed layer. Kink instabilities instead result in a thicker field-reversed state with many non-axis-encircling particles. The final state appears to be stable but with higher electric fields and substantial electron currents.

---

1. R.V. Lovelace, Phys. Fluids 22, 708 (1979).

Instability Thresholds				
v_A/c	η_s			
	n=2	n=3	n=4	n=5
.00250	0.4	2.2	5.0	8.5
.00125	1.0	4.2	8.0	12.0
.000625	1.8	5.0	9.5	15.0
.0003125	2.0	6.0	11.0	18.0

TBL. 1. Instability threshold values of the self-magnetic field index.

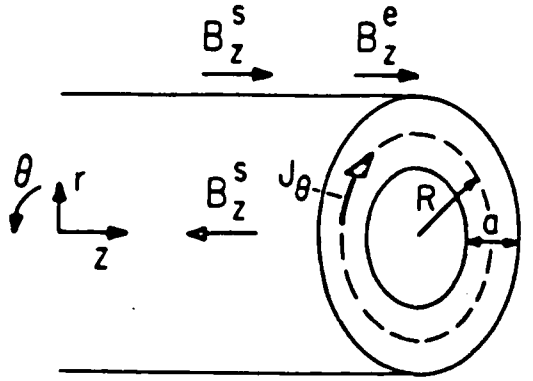

FIG. 1. Schematic of an infinitely long field-reversing ion layer.

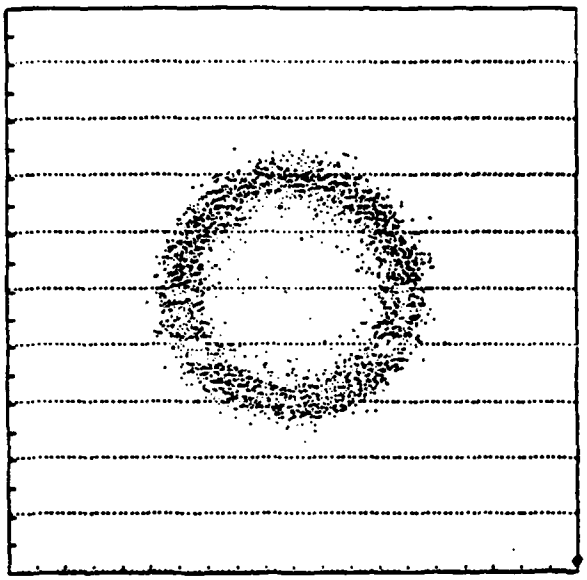

FIG. 2. Initial particle positions in the $r-\theta$ plane for an ion layer with $\zeta=1.32$.

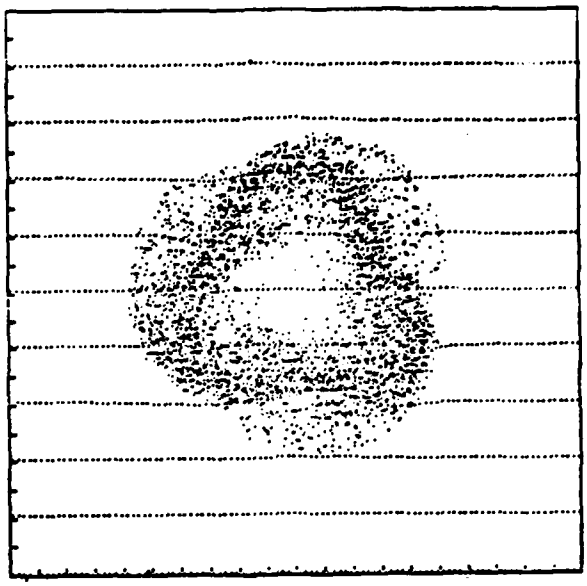

FIG. 3. Particle positions after ten ion-cyclotron periods. An $n=3$ instability has grown to a large amplitude and nonlinear effects have become important.

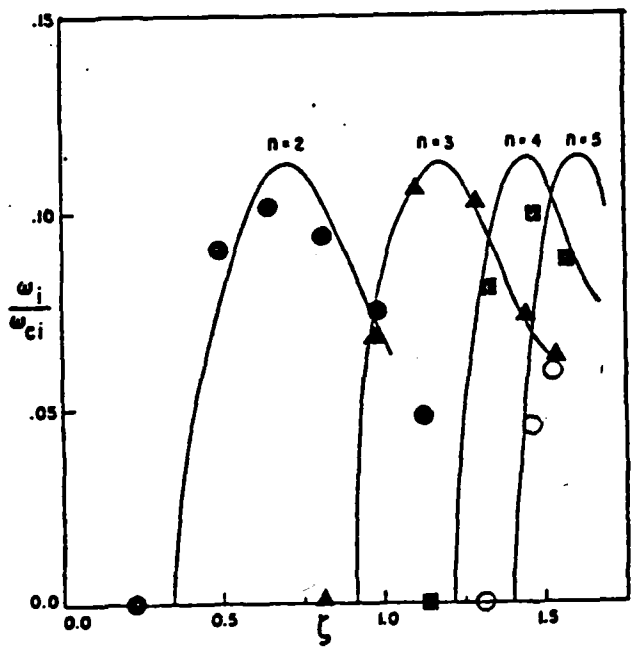

FIG. 4. Growth rates, ω_i, for ion layers with $(R/a)\approx 5$ and $(v_A/c)=.00125$ as a function of the loading factor. (● $n=2$, ▲ $n=3$, ■ $n=4$, ○ $n=5$).

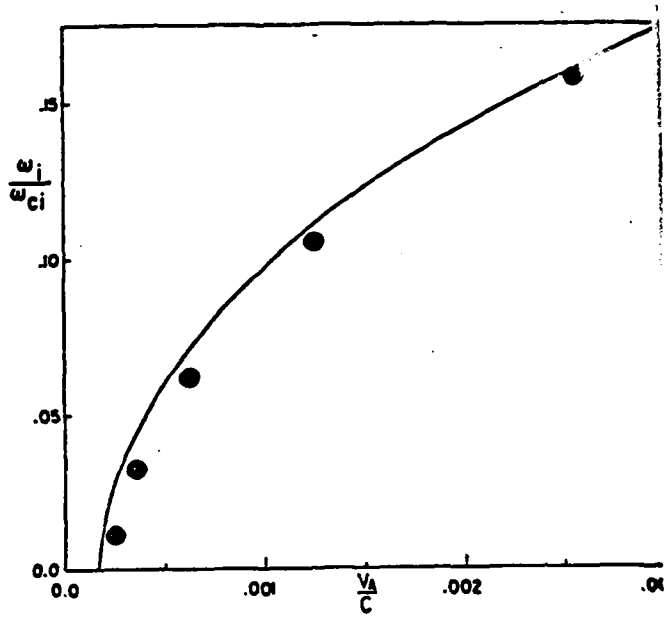

FIG. 5. Growth rates of $n=2$ modes for ion layers with $(R/a)\approx 5$ and $\zeta=.65$ as a function of background plasma Alfven speed.

Section II

CODE DEVELOPMENT AND MAINTENANCE

A. *Implicit Particle Simulation using Moments with Orbit Averaging*

V. Thomas (Dr. B. I. Cohen LLL and Prof. C. K. Birdsall)

A first attempt at including orbit averaging in electrostatic implicit moment particle simulations has failed. The motivation for attempting to include orbit averaging in a moment implicit code is for the improvement of particle statistics. (See the previous QPRs for implicit moment simulation references and orbit averaging references.) The algorithm is shown in Figure 1. Starting at time $N\Delta T$ with E^{N+1}, we advance the particles from $N\Delta T$ to $(N+1)\Delta T$. Then we use the current density averaged over the micro steps from $(N-1/2)\Delta T$ to $(N+1/2)\Delta T$ and the charge density averaged over the microsteps from $N\Delta T$ to $(N+1)\Delta T$ to predict the charge density at time $(N+3/2)\Delta T$ via

$$\tilde{\rho}^{N+3/2} = \{\rho\}^{N+1/2} - \frac{\partial}{\partial x}\tilde{j}^{N+1}\Delta T \tag{50}$$

and

$$\tilde{j}^{N+1} = \sum_{\alpha}\left[\{j_\alpha\}^N - \frac{q_\alpha}{m_\alpha}\left(\frac{\partial}{\partial x}\{P_\alpha\}^{N+1/2} - q_\alpha\{n_\alpha\}^{N+1/2}E^*\right)\Delta T\right] \tag{51}$$

the brackets indicate orbit averaging and the tilde indicates a predicted quantity. P is the pressure, alpha is the species label, E^* is a linear combination of E^N , E^{N+1}, and E^{N+2} , and n represents the particle density. The field at time $(N+2)\Delta T$ is solved for implicitly by

$$-(1-\epsilon)\nabla^2\phi^{N+2} - \epsilon\nabla^2\phi^{N+1} = \tilde{\rho}^{N+3/2} \tag{52}$$

where $\tilde{\rho}^{N+3/2}$ is predicted from the first two equations. ϵ is a biasing parameter intended to control dissipation.

This algorithm is unstable , even for small time steps. We are working to understand the results and we are persuing alternatives.

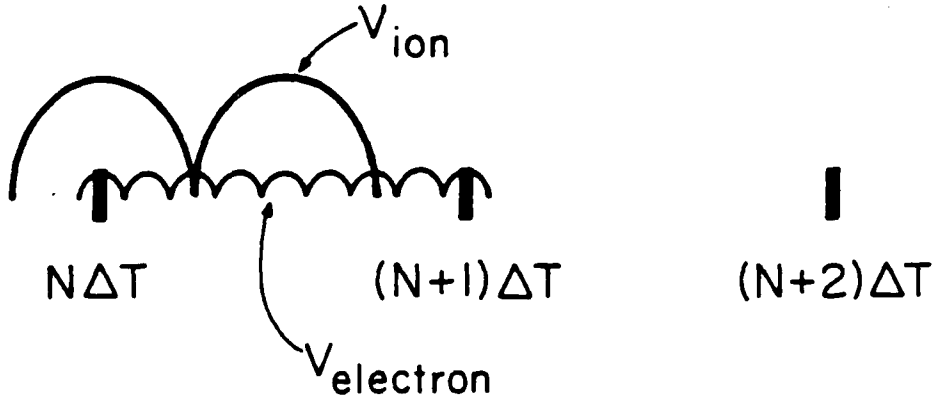

Figure 1. Using E^{N+1} the ions and the electrons are advanced on possibly different time steps up to the time $(N+1)\Delta T$. Then E^{N+2} is solved for implicitly and the cycle repeats.

B. A NEW METHOD FOR IMPLICIT PARTICLE SIMULATION

Alex Friedman*, A. Bruce Langdon**, and Bruce I. Cohen**

The following is a brief account of our recent work on implicit methods for particle simulation. The algorithm we describe, named BAAL (for Bay Area ALgorithm), was developed during the final quarter of 1980, while one of us (A.F.) was a postdoctoral associate with the U. C. Berkeley Plasma Theory and Simulation Group. This work, which has application to both inertial and magnetic confinement fusion plasma simulation, is continuing at the Lawrence Livermore National Laboratory, with continuing close ties to the U. C. Berkeley group.

The first section below (written primarily by A.B.L.) has been excerpted from our contribution to the 1980 LLNL Laser Fusion Annual Report. It provides an overview of our work, and describes an ideal (gridless) form of the algorithm. The second section below briefly describes the cloud-in-cell algorithm used in the testbed code developed at U. C. Berkeley. The final section presents some illustrative results. Details of this work, other forms of the BAAL algorithm, and our analyses of the time-differencing algorithms will be presented in future publications.

*Present affiliation: Lawrence Livermore National Laboratory

**Affiliation: Lawrence Livermore National Laboratory

I. Ideal Algorithm

We have made several advances in the quest for more efficient simulation of low-frequency plasma phenomena. Our most adaptable and reliable tools for study of kinetic plasma behavior are the "particle" codes, but the stability of these codes has previously required resolution of the electron plasma period in the time integration, even when the phenomenon under study took place on the much-longer ion time scale.

Analogous limitations on time step in other problems, such as heat flow and chemical rate equations, are overcome through the use of *implicit* time integration schemes. In particle codes, although implicit methods have been analyzed theoretically,[1] their application has been inhibited by the very large number of nonlinear equations to be solved simultaneously, about equal to the number of particle coordinates plus the number of zone quantities (electric and magnetic fields).

We have begun to experiment with a new method for solution of these equations in two steps. In this method, equations are first set up for the fields. Although these equations involve information from the particles, the number of equations to solve simultaneously is only the number of field quantities, defined on the zones. Since the number of zones is much less than the number of particles, and the resulting matrix equations are sparse and well conditioned, their solution is convenient with known methods. Once the fields are known, the particle

coordinates can be readily solved for serially, one particle at a time. Here, we will discuss simulations having only the electrostatic field.

First we consider finite-differenced equations of motion for the particles which have the necessary stability at large time-step and are accurate for the low frequency phenomena to be studied. In Ref. 3, a centered expression for the time derivative is employed. Use of this expression leads to a numerically stable algorithm at large $\omega_p\Delta t$, but by itself does not damp high frequency components of the motion, which are aliased into the Nyquist frequency - stable odd-even oscillations of large amplitude can persist. In Ref. 2, the derivatives are biased using a scheme such as

$$v_{n+1}-v_n = \left(\tfrac{3}{4}a_{n+1}+\tfrac{1}{4}a_{n-1} \right)\Delta t \qquad (1a)$$

$$x_{n+1}-x_n = \left(\tfrac{3}{4}v_{n+1}+\tfrac{1}{4}v_{n-1} \right)\Delta t \qquad (1b)$$

This scheme damps unwanted high-frequency oscillations, while low frequencies are very weakly damped, as desired: $(\mathrm{Im}\omega)/\omega=\mathcal{O}(\omega\Delta t)^3$. Such schemes are members of a class whose application to plasma simulation has been analyzed in detail in Ref. 1 and in our present work. We have also devised a different class of schemes, whose simplest member is

$$2\left(v_{n+1/2}-v_{n-1/2} \right) - \left(v_{n-1/2}-v_{n-3/2} \right) = a_{n+1}\Delta t \qquad (2a)$$

$$x_{n+1}-x_n = v_{n+1/2}\Delta t \qquad (2b)$$

This scheme has the same order of accuracy as Eq. (1), while requiring less storage of time levels. The presence of the acceleration at only the n+1 time level increases the damping of high-frequency oscillations. The optimum design of these difference equations is the first issue in practical implementation of large time-step methods.

In all implicit schemes the new positions x_{n+1} depend on the accelerations a_{n+1} due to the electric field E_{n+1}. But this field is not yet known, as it depends on the density ρ_{n+1} of particle positions $\{x_{n+1}\}$. The solution of these coupled particle and field equations is the other major implementation issue.

In the method developed by Denavit[2] and Mason[3] for this solution, the fields at the new time level are predicted by solving coupled field and fluid equations, in which the pressure tensor is approximately evaluated from particle velocities known at the earlier time. After the fields are known, the particles are advanced to the new time-level, and, if desired, an improved pressure tensor is calculated and the process iterated.

It is also practicable to predict the future electric field E_{n+1} quite directly by means of a linearization of the particle-field equations. Since this method and its implementation in the experimental code BAAL have not been described previously, we outline the concept here.

The position x_{n+1} of a particle at time level t_{n+1}, as given by an implicit time integration scheme, can be written as

$$x_{n+1} = \beta\Delta t^2 a_{n+1} + x_{n+1}^{(0)}, \tag{3}$$

where $0<\beta\leq 1$ and $x_{n+1}^{(0)}$ is the position obtained from the equation of motion with the acceleration a_{n+1} neglected. Since $x_{n+1}^{(0)}$ depends only on positions and accelerations at times t_n and earlier, it is known. In its simplest form, the BAAL algorithm is derived by linearization of the particle positions relative to $x_{n+1}^{(0)}$.

One can regard the actual position, x_{n+1}, as $x_{n+1}^{(0)}$ plus a displacement $\delta x = \beta\Delta t^2 a_{n+1}$. We form a charge density $\rho_{n+1}^{(0)}$ from $\{x_{n+1}^{(0)}\}$; the actual charge distribution is then $\rho_{n+1}^{(0)}$, plus the change $\delta\rho$ brought about by displacing particles by the amount $\delta x = x_{n+1}-x_{n+1}^{(0)}$. Linearized, this increment to ρ is[1]

$$\delta\rho = -\nabla\cdot[\rho_{n+1}^{(0)}(x)\delta x(x)] \tag{4}$$

To the same order of approximation, the displacement $\delta x(x)$ of all particles with $x_{n+1}^{(0)} \cong x$ is obtained with a_{n+1} evaluated at x, i.e.

$$\delta x(x) \cong \beta\Delta t^2 (q/m) E_{n+1}(x) \tag{5}$$

We then have

$$\delta\rho(x) = -\nabla\cdot[\chi(x)E_{n+1}(x)] \tag{6}$$

where the effective susceptibility is

$$\chi(x) = \beta[\rho_{n+1}^{(0)}(x)q/m]\Delta t^2 = \beta\omega_p^2(x)\Delta t^2 \tag{7}$$

Note that χ depends only on the particle positions $\{x_{n+1}^{(0)}\}$, and not at all on velocity information as required in the moment equation methods.

With these two source contributions, the Poisson equation becomes, in rationalized c.g.s. units,

$$\nabla\cdot E_{n+1} = \rho_{n+1}^{(0)} - \nabla\cdot(\chi E_{n+1}) \tag{8}$$

or

$$-\nabla\cdot[1+\chi]\nabla\varphi_{n+1} = \rho_{n+1}^{(0)} \tag{9}$$

This elliptic equation is solved by standard methods. The field $-\nabla\varphi_{n+1}$ and (5) are then used to calculate the positions $\{x_{n+1}\}$. This algorithm is reminiscent of the method for solution for the vector potential A in some magneto-inductive plasma simulation codes.[4,5]

Should it be necessary, we have shown how to refine the approximations used above by: linearization about a more accurate prediction of x_{n+1} than $x_{n+1}^{(0)}$, iteration, and a more accurate evaluation of δx.

In our spatial-difference representation of these equations, Eq. (4) becomes the gradient of a zonal ρ with respect to particle position, and δx in Eq. (5) depends on the electric field in two zones, using the usual interpolation. In this way we are assured that the density ρ_{n+1} of final particle positions $\{x_{n+1}\}$ satisfies the code's representation of the Poisson equation, $-\nabla^2\varphi_{n+1} = \rho_{n+1}$, so that desirable features built into the time-differencing scheme will be realized in practice.

We are delineating the limitations of implicit methods and learning how to surmount them. For example, it is observed that an unphysical cooling of the electrons occurs when uncentered equations of motion are used. Our analysis provides guidance to design algorithms which retain desirable dissipation of high-frequency oscillations while minimizing this unwanted cooling. This side effect is related to the damping of *low* frequency oscillations; both are smaller in our schemes above with third-order damping than in lower-order algorithms.[3]

To date, the BAAL approach has been verified in application to ion acoustic oscillation and two-stream instability, with $\omega_p\Delta t$ in the range 2.5 - 4.0. Numerical stability and correct dispersion of the testbed code have been verified for a cold simulation plasma up to $\omega_p\Delta t = 25$.

II. Cloud-in-Cell Algorithm

The testbed computer simulation program we have developed, BAAL, employs well-known particle-in-cell techniques to assure a smooth interpolation of the zonal electric field onto the particle locations and of the particle charge onto the charge-density grid. We illustrate the scheme with a fully-implicit (backward differenced) model algorithm; the actual code is far more general.

In the model algorithm, each particle k is advanced via:

$$v_k^{m+1} = v_k^m + (q/m)\Delta t E^{m+1}(x_k^{m+1}) \tag{10a}$$

$$x_k^{m+1} = x_k^m + \Delta t v_k^{m+1}. \tag{10b}$$

For each cell j, we write the charge density as:

$$\rho_j^{m+1} = (q/\Delta x)\sum_k S(x_k^{m+1} - x_j), \tag{11}$$

where the "shape function" S is the finite-size particle analogue of the Dirac delta function, and the sum is taken over all particles k which overlap cell j to any degree. The calculation of E^{m+1} requires knowledge of ρ^{m+1} before we have explicit knowledge of the x_k^{m+1}. In essence, the BAAL algorithm calculates this charge density implicitly by approximating it as a linear function of E^{m+1}. We compute a simple approximation $\tilde{x}_k$ (this is $x_{n+1}^{(0)}$ of the previous section) to x_k^{m+1} via:

$$\tilde{x}_k = x_k^m + \Delta t v_k^m, \tag{12}$$

which for this simple model is just a "free-streaming" location. We expand the shape function in a Taylor series:

$$S(x_k^{m+1}-x_j) \approx S(\tilde{x}_k-x_j) + (x_k^{m+1}-\tilde{x}_k)\partial S(\tilde{x}_k-x_j)/\partial \tilde{x}_k, \tag{13}$$

and note that the expansion is exact for linear-spline particles which do not cross cell boundaries as a result of the new acceleration, i.e. which intersect the same cells at x_k^{m+1} and $\tilde{x}_k$. We approximate the coefficient of the first-derivative term via

$$\begin{aligned} x_k^{m+1}-\tilde{x}_k &= (q/m)\Delta t^2 E^{m+1}(x_k^{m+1}) \\ &\approx (q/m)\Delta t^2 \sum_i S(\tilde{x}_k-x_i)E_i^{m+1}, \end{aligned} \tag{14}$$

with a relative error of order $\omega_{Trap}^2 \Delta t^2 = qE\Delta t^2/mL_{scale} << 1$, where L_{scale} is a typical scale length over which E varies. This approximation imposes a limitation (shared by the moment-equation method) on L_{scale} and $|E|$ for the simulation to be valid. We are considering modifications to the algorithm which may eventually allow us to relax this restriction.

Using Eqns. (11), (13), and (14), the field equation solved is:

$$(\nabla \cdot E)_j = \rho_{j(conv)} + \sum_i W_{ij} E_i, \tag{15}$$

where the "conventional" charge density is:

$$\rho_{j(conv)} = \sum_k qS(\tilde{x}_k - x_j), \tag{16}$$

and the "weights" W_{ij} couple each cell to its neighbors when particles are present:

$$W_{ij} = (q^2\Delta t^2/m)\sum_k S(\tilde{x}_k - x_i)\partial S(\tilde{x}_k - x_j)/\partial \tilde{x}_k. \tag{17}$$

For linear splines $W_{ij}=0$ whenever $|i-j|>1$. Since for linear splines $\partial S/\partial \tilde{x}_k = \pm 1/\Delta x$ (or zero), there is considerable redundancy in the calculation of the $\rho_{j(conv)}$ and the W_{ij}, and it turns out that (at least for the unmagnetized 1d electrostatic code) the number of operations needed to weight all necessary quantities to the grid is the same as the number needed in the conventional ES1 code. Since the field interpolation and charge deposition steps tend to dominate the particle processing time on a vector computer like the Cray-1, the algorithm is potentially very efficient.

At present, the field equation is written in terms of the electrostatic potential φ, and is solved by successive overrelaxation. Direct solution is more difficult to generalize to higher dimensional problems. Spatial filtering is provided for through use of a fast Fourier transform on the potential obtained after the field equation has been solved.

III. Code Results

As a first check of code performance, we initialized a cold electron plasma (with immobile ions) in a run with parameters ω_p=1.0, Δt=10.0 (run "CLD2"). For this run, the BAAL testbed used a time-centered version of the model difference scheme described in this section. Thirty-two cells, and 128 particles, were employed, and there was an initial excitation of mode 1 (the longest wavelength mode). Figure (1) shows a "history" of the energy in this mode as a function of time. An oscillation with a period of 160 is clearly evident in the figure. What is not evident is that the oscillation is in fact a modulated odd-even oscillation in time, i.e. with a frequency differing from the Nyquist frequency $\pi/\Delta t$ by only the small shift $\delta\omega=2\pi/160$. To understand this, we observe that the dispersion relation for this "trapezoidal rule" scheme is:

$$2/\omega_p\Delta t = \cot\ \omega\Delta t/2 \qquad (18)$$
$$= \tan\ (\pi/2 - \omega\Delta t/2),$$

Thus, the mode frequency

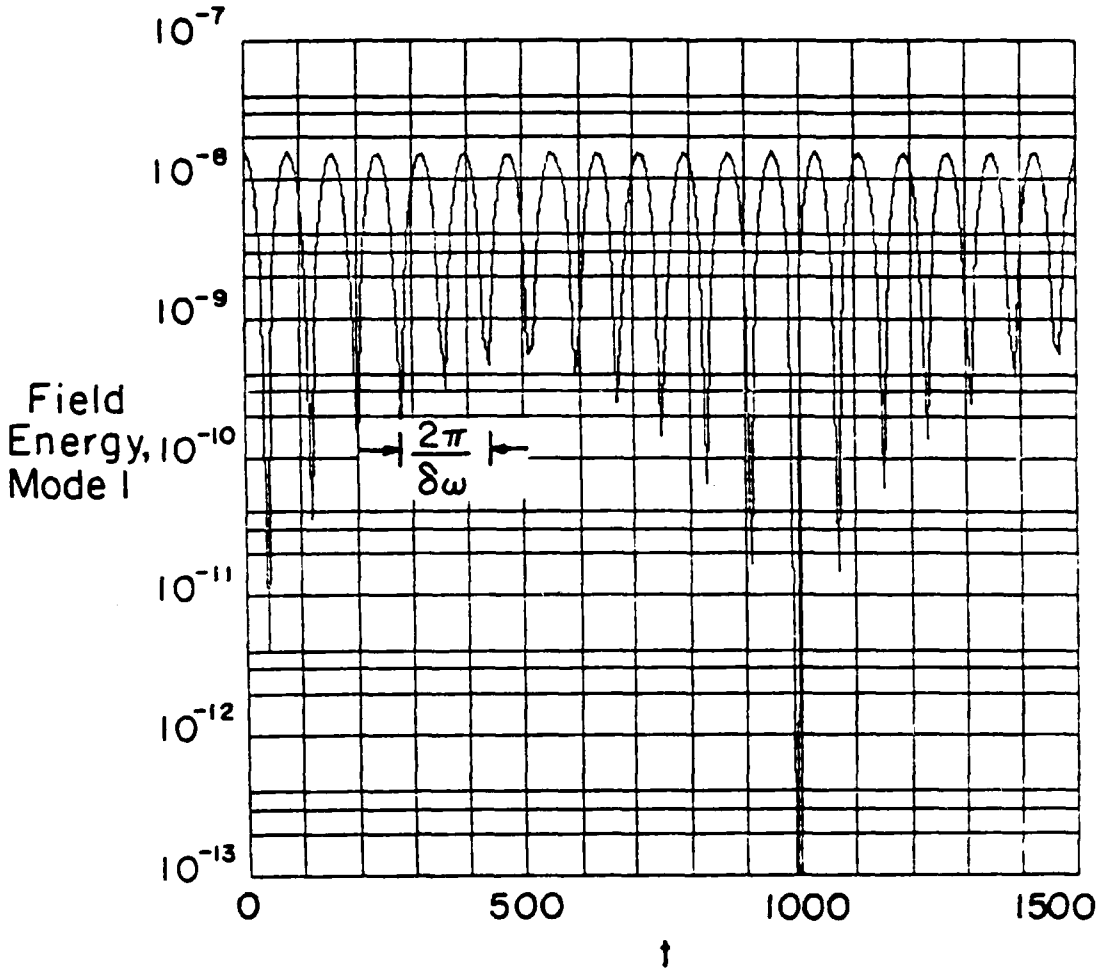

Fig. 1 Mode 1 energy versus time for cold plasma oscillation run CLD2.

$$\omega \approx \pi/\Delta t - 4/\omega_p \Delta t^2, \tag{19}$$

so that the frequency shift is $\delta\omega = 4/\omega_p \Delta t^2 = 0.04$ leading to a period of 157. Similar behavior was observed for Δt=25.0.

When the difference scheme of Eqn. (1) is employed, the odd-even oscillations (aliased plasma wave) are observed to damp out rapidly, with $\gamma_{obs} \approx -0.07$. This compares well with the predicted damping factor $\gamma_{pred} = -0.069$. Similar damping is obtained when "stiffly stable" schemes such as that of Eqn. (2) are employed.

As a first model problem, we consider the electron-electron two-stream instability arising from the relative motion of two cold beams of infinite spatial extent. The first run made, "EE00", was a benchmark, using the conventional ES1 leapfrog simulation algorithm and a small timestep, Δt=0.25 with ω_p(total)=1.0. For this run, a grid of 32 cells was employed, and 128 particles were used to represent each beam. No spatial filtering was employed (the capability had not yet been implemented), and thus the fastest growing mode was that with the shortest wavelength, mode number 16. Figure (2) is a plot of the field energy as a function of time for this run; the analytically predicted growth rate for the parameters chosen, normalized to the plasma frequency, is γ_{pred}=0.31, while the observed growth rate is γ_{obs}=0.29. Thus, despite the fact that the mode in question has a wavelength of only two cells, there is good agreement with simple theory.

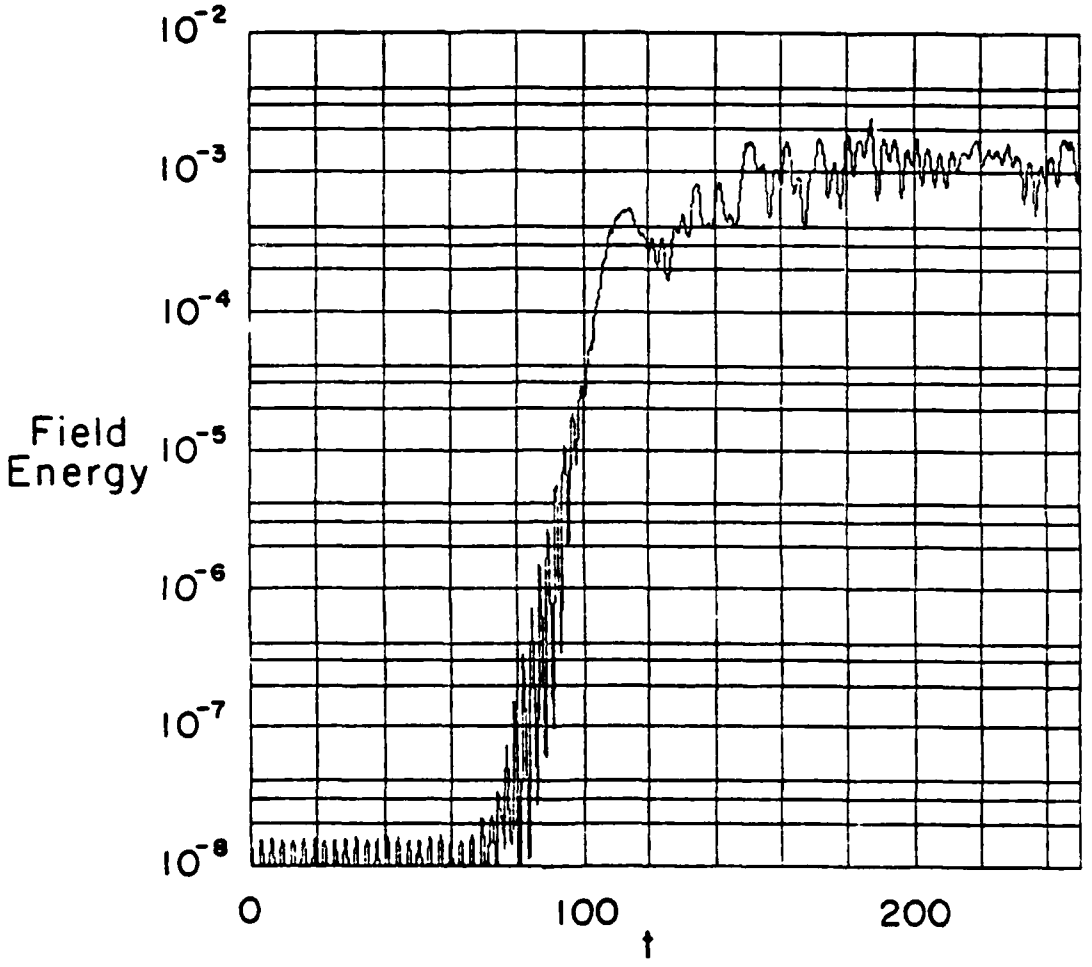

Fig. 2 Field energy versus time for benchmark e-e two-stream run EE00.

For comparison with the above run, another ("EE03") was made using the BAAL testbed code. The timestep was ten times as large, $\Delta t=2.5$, and a time-centered version of the model algorithm of this section was employed. Thus, there was no damping of the aliased plasma oscillations at the Nyquist frequency (these would not be visible in a field energy plot anyhow, since only the square of the electric field enters into that diagnostic). The results of this run are shown in Fig. (3). The instability is not evident until a later time in the BAAL simulation; presumably this is due to a smaller initial level of excitation of the unstable mode. Once visible growth begins, it is clear that the growth rates in this run and the previous run are very nearly equal, while the saturation level in the implicit code run is only slightly lower than that of the ES1 run. There is thus good agreement with both simple theory and the benchmark run, despite the poor resolution of the mode in question on the grid.

As a second model problem[6], we consider an ion-acoustic traveling wave, with $\omega_{pe}=1.0$, $\Delta t=3.0$ (run "IA04"). For this run, the time-level biasing of Eqn. (1) was employed, as was a spatial filtering which discarded all but modes 1-4, and which filtered modes 3 and 4 rather heavily. Mode 2 was excited, there were 128 grid cells, the mass ratio m_i/m_e was 16, and there were 2048 electrons and 512 ions. The system length L was 16π, the electron thermal velocity $v_{th,e}$ was 0.25 (the ions were cold), the Debye length λ_D was 0.25, and the wave vector k was 0.25. The sound speed c_s was 0.0645, and the wave frequency ω was 0.0161

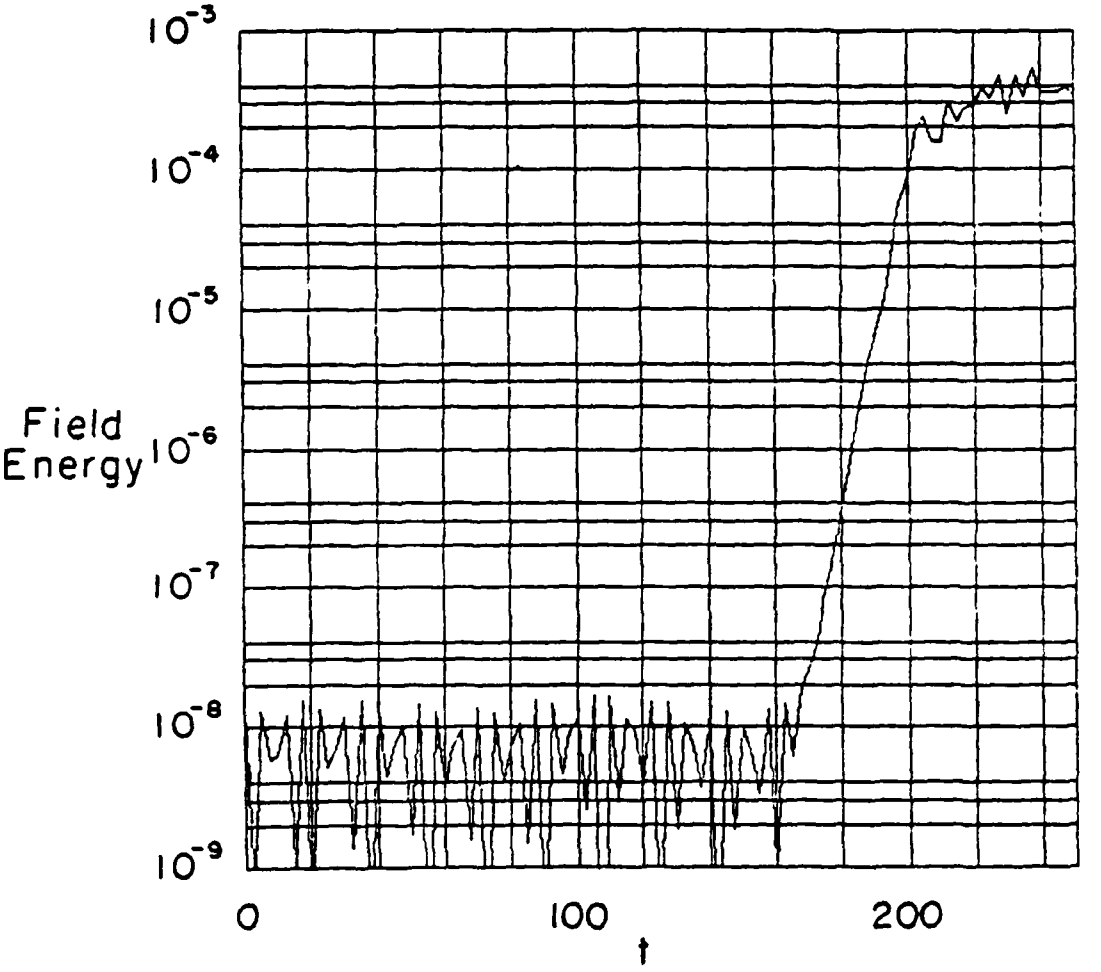

Fig. 3. Field energy versus time for BAAL two-stream Run EE03.

leading to a period τ of 390. Figure (4) is a "snapshot" of the smoothed ion density as a function of x at the beginning of the run. The corresponding quantity at time t=210 (slightly more than half a wave period later) is shown in Fig. (5). One predicts that the lefthand peak should have moved $210c_s$=13.59 units during this period of 70 timesteps, and measures a traveled distance of 19.3-6.1=13.2. Thus, the phase velocity of the wave is essentially correct. At later times mode 4 comes up out of the noise and the clean structure visible in these snapshots disappears.

We have successfully modeled ion acoustic standing waves with mass ratios up to 1600 and timesteps Δt as large as $4.0.^7$ Up to 6000 timesteps have been employed in these runs, which are "noisier" than the one described above despite the fact that only a single mode was allowed.

Our future plans include the modeling of warm two-stream instabilities wherein the physically fastest-growing mode is well resolved in the simulation, and the verification of the correct behavior of a plasma expanding into vacuum. Practical application of these methods to problems in inertial and magnetic confinement fusion will be forthcoming.

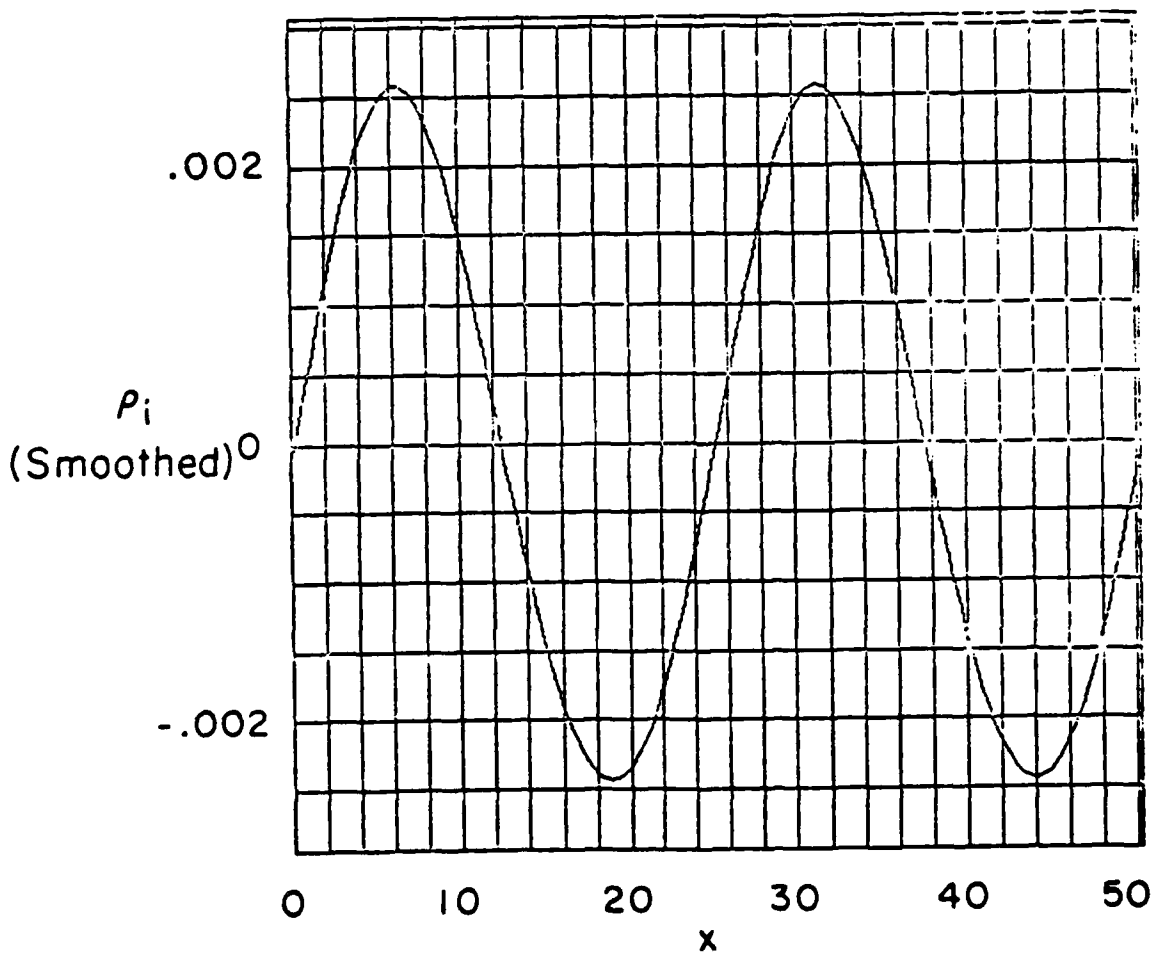

Fig. 4. Initial smoothed ion density versus x for ion-acoustic wave run IA04.

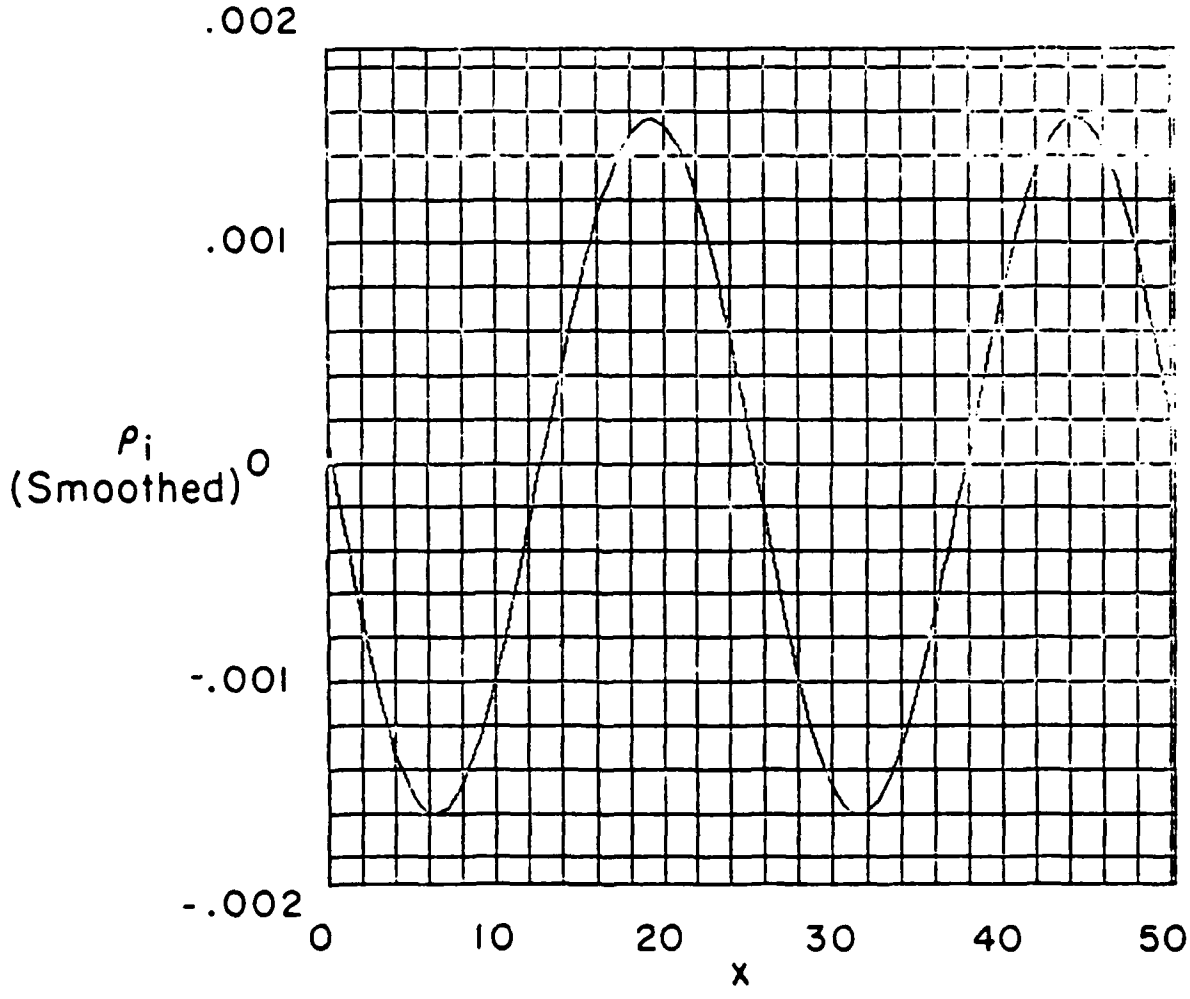

Fig. 5. Smoothed ion density versus x at time 210 for run IA04.

REFERENCES

1. A. Bruce Langdon, *J. Comput. Phys.* 30, 202 (1979).

2. J. Denavit, "*Time Filtering Particle Simulations with* $\omega_{pe}\Delta t >> 1$", UCRL-85097, to appear in *J. Comput. Phys.*

3. R. J. Mason, "*Implicit Moment Particle Simulation of Plasmas*", to appear in *J. Comput. Phys.*

4. A. Friedman, R. L. Ferch, R. N. Sudan and A. T. Drobot, *Plasma Phys.* 19, 1101 (1977); A. Mankofsky, A. Friedman and R. N. Sudan, "*Numerical Simulation of Injection and Resistive Trapping of Ion Rings*", to appear in *Plasma Phys.*

5. D. O. Dickman, R. L. Morse and C. W. Nielson, *Phys. Fluids* 12, 1708 (1969).

6. The parameters for this run were suggested by D. Potter.

7. The parameters for this series of runs were suggested by V. Thomas.

C. *POLARES*

Niels F. Otani (C. K. Birdsall)

The master-slave structure of the POLARES code described in the last QPR is now in place, although rough spots still remain. We find the new code reproduces results obtained from the old code. The predicted graphics flexibility appears to have been realized, though some bugs remain. Also difficulty has been encountered in the organization of the history file, and corresponding portions of the code will probably have to be rewritten. Restart and negative timestep capabilities (see previous QPR) have not been installed but the prospect of their successful implementation remains promising.

We have learned from A. B. Langdon (private communication) that the master-slave organization used in this code is not the most efficient since the code must generally wait to regain core each time a switch between master and slave is made. In this regard and also from the point of view of ease in coding, the use of overlays probably would have been preferable. However, the present format, having already been written, will be maintained.

D. *Solver Updates*

H. Stephen Au-Yeung

(1) New Parameters

Several new parameters have been added to SOLVER to allow the user to override the labels and to override the lower and upper bound of the graph; they are:

Hori	Horizontal label.
Vertre	Vertical label for the real part.
Vertai	Vertical label for the imaginary part.
Headre	Heading label for the real part.
Headai	Heading label for the imaginary part.
Xmin	Lower bound of x.
Xmax	Upper bound of x.
Remin	Lower bound of the real part of the root.
Remax	Upper bound of the real part of the root.
Aimin	Lower bound of the imaginary part of the root.
Aimax	Upper bound of the imaginary part of the root.
Wmin	Lower bound of the second argument w.
Wmax	Upper bound of the second argument w.

(2) Get around the limitation of 1024 points for function plotting

When plotting a function vs. one argument, one could plot as many as 2048 points by specifing the following in the input file of tty:

nx=2048 nw=1

E. *Quiet Start Method Comparisons; Random, Bit Reversed, and Fibonacci Numbers*

H. Stephen Au-Yeung, and Yu-Jiuan Chen (Prof. C.K. Birdsall; Dr.

A.B. Langdon, LLL)

Quiet starts for Maxwellian distribution [or other $f(v)$ or $n_o(x)$] use some set of uniform numbers for inverting the cumulative distribution function. The set may be regular or other. We have chosen to make some comparisons among sets stimulated in part by the work of *Denavit and Walsh* (1980) using Fibonacci numbers based on that of *Wick* (1979, 1980).

An earlier method used by A.B. Langdon in ES1, subroutine INIT (since June 1978) is to invert $f_o(v)$ using uniform numbers from slow to fast, hence highly correlated, and then to scramble positions [$n_o(x) = constant$] in order to reduce correlations using a bit reversed method.

The main reason for using the quiet start loader is to reduce the noise level. The noise will be increased by particle bunching. Therefore, we decided to compare the uniformity of the numbers generated by the Fibonacci number method, the bit reversed method, and computer (CRAY-1) generated random numbers. Keep in mind that uniformity (lack of bunching) is not the only test, as correlations that excite various (ω,k) preferentially are also unwanted; tests of the latter kind have not been made as yet.

Fibonacci numbers are defined as

$$\alpha_{n+1} = \alpha_n + \alpha_{n-1}\,, \qquad n = 1,2,\cdots \tag{1}$$

with $\alpha_0 = \alpha_1 = 1$. The sequence is 1, 1, 2, 3, 5, 8, 13, etc. Following Wick, we use N particles with $N = \alpha_n$ to attempt to fill a unit square uniformly by using

$$x_i = \frac{i - \frac{1}{2}}{\alpha_n}\,, \quad y_i = \left[\frac{(i-1)\alpha_{n-1} + \frac{1}{2}}{\alpha_n}\right]_{mod\ 1}\,, \quad i = 1,\cdots,N{=}\alpha_n \tag{2}$$

where (x_i,y_i) is the location of the i^{th} particle. Figure 1 has (x,y) scatter plots for $N = 233$, 377, 610, 987, 1597, 2584, 4181, and 6765. There is no mystery here; the x_i's step across slowly and the y_i's step up rapidly, both uniformly, creating the 2d space lattices shown. The resolution of these patterns required photo printing (fiche); if done on the Versatec, with less resolution, spurious bunching resulted, sort of Moire patterns. The Fibonacci method clearly produces highly correlated (x,y). For example, suppose the particles were allowed to free stream as

$$x' = x - yt \quad \text{modulo 1}$$

$$y' = y$$

treating y like velocity. Using $N = 987$, note that at $t \approx 1$, there will be roughly 21 nearly perfect vertical bars, such that if (x,y) were (x,v_x) there would be a large density produced in mode 21, defeating the purpose of the quiet start. At other values of t, other Fibonacci "crystals" will "resonate" similarly.

For the bit-reversed method, we set $N = 2^n$ where n is an integer. The x_i are chosen as before, with $x_i = (i + \frac{1}{2})/N$, with i running 0 to $N-1$. The y_i are chosen using the bit-reversed algorithm in ES1 plus a $1/2N$. The scatter plots are shown in Figure 2, for $N = 64$, 128, 256, 512, 1024, 2048, 4096, and 8192. This method appears to our eyes to avoid correlations in small (x,y) regions (no obvious lattice) although there are a few closely spaced $(x-y$'s). (There appears to be symmetry about $\pm 45°$.) Hence, the resonance possibility or magnitude appears less here.

Bit reversed fractions were not familiar to us, so a short explanation and algorithm is given here. The table below makes bit reversed fractions from the binary equivalent of the x_i's.

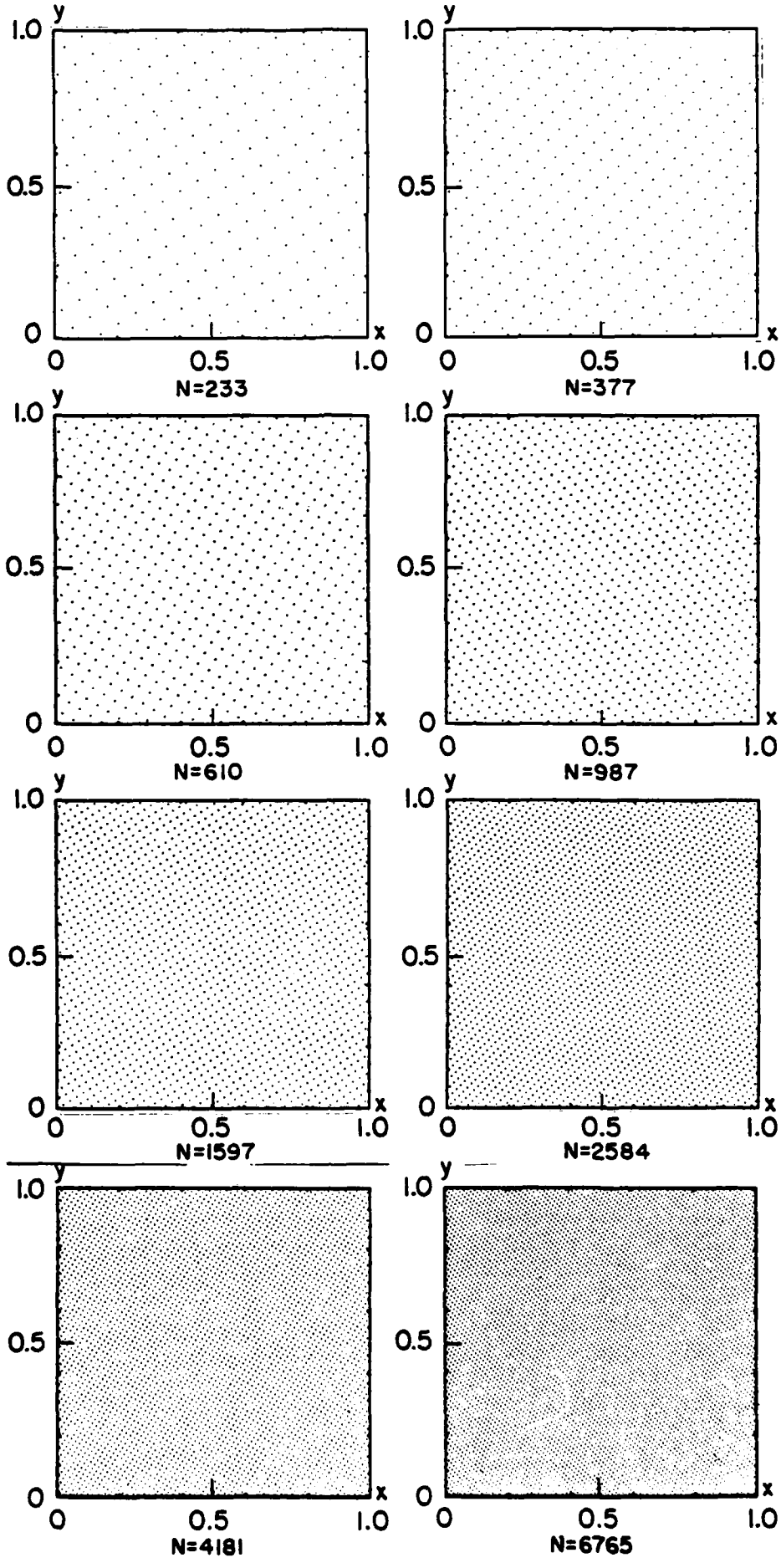

Figure 1. x_i, y_i space with the y_i chosen from a Fibonacci number ratio.

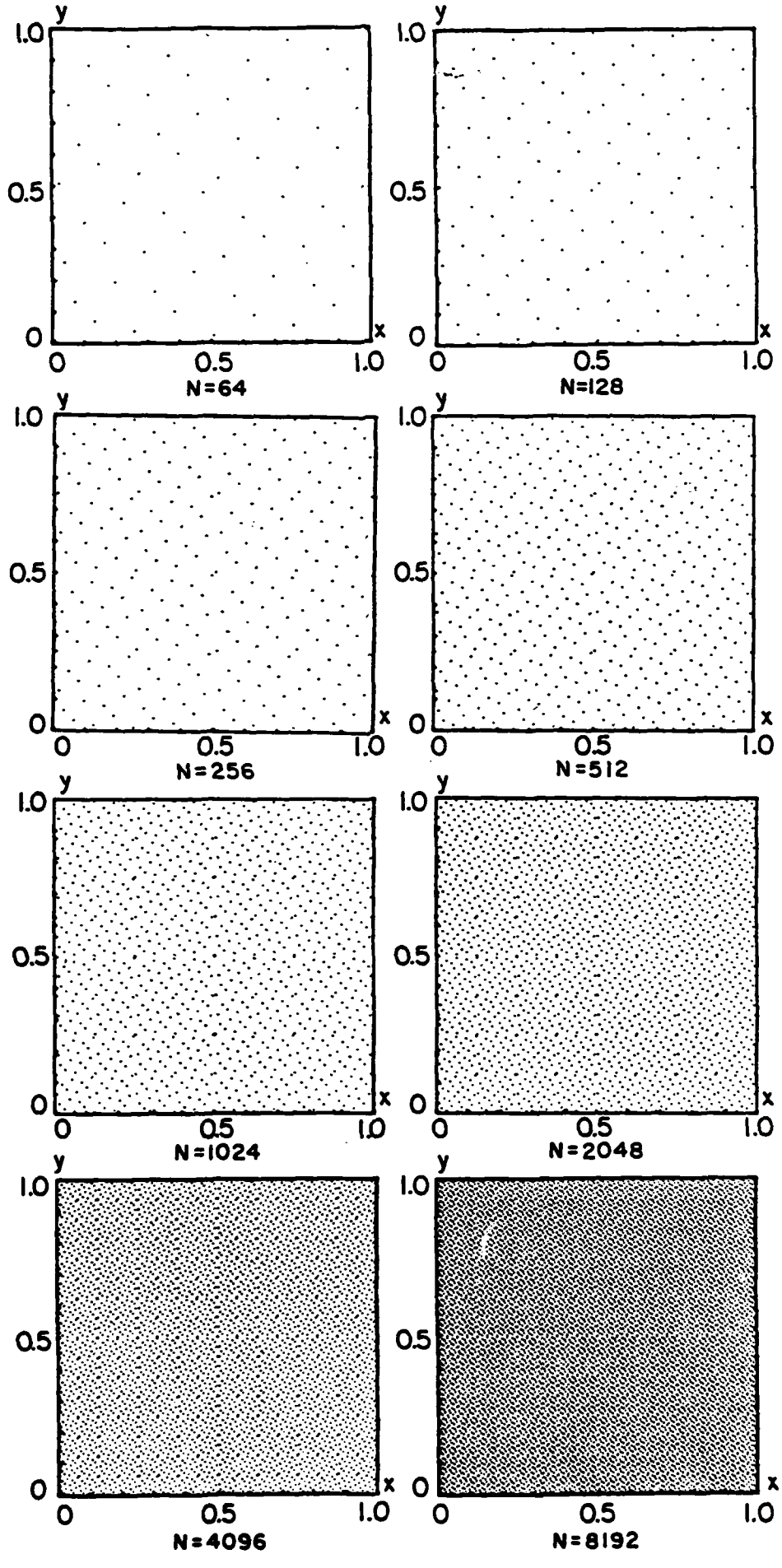

Figure 2. x_i, y_i space with the y_i chosen from a bit reversed sequence.

n	N	Decimal	Binary	Binary reversed	Fraction
0	1	$x_0 = 0$	0.	.0	$y_0 = 0$
1	2	$x_1 = 1$	1.	.1	$y_1 = 1/2$
		$x_2 = 2$	10.	.01	$y_2 = 1/4$
2	4	$x_3 = 3$	11.	.11	$y_3 = 3/4$
		$x_4 = 4$	100.	.001	$y_4 = 1/8$
		$x_5 = 5$	101.	.101	$y_5 = 5/8$
		$x_6 = 6$	110.	.011	$y_6 = 3/8$
3	8	$x_7 = 7$	111.	.111	$y_7 = 7/8$
		$x_8 = 8$	1000.	.0001	$y_8 = 1/16$
		$x_9 = 9$	1001.	.1001	$y_9 = 9/16$
		$x_{10} = 10$	1010.	.0101	$y_{10} = 5/16$
		$x_{11} = 11$	1011.	.1101	$y_{11} = 13/16$
		$x_{12} = 12$	1100.	.0011	$y_{12} = 3/16$
		$x_{13} = 13$	1101.	.1011	$y_{13} = 11/16$
		$x_{14} = 14$	1110.	.0111	$y_{14} = 7/16$
4	16	$x_{15} = 15$	1111.	.1111	$y_{15} = 15/16$
5	32	16 - 31	10000. - 11111.	.00001 - .11111	1/32 - 31/32
6	64	32 - 63	100000. - 111111.	.000001 - .111111	1/64 - 63/64

The values of y used in ES1 are those in the table plus $1/2N$. A readable code for producing the bit reversed ($y_i + 1/2N$) follows.

```
      integer   Num, n, K, KthBit, TwoToK
      real      B
      namelist  /in/  n
c
c Read in n
c
      read(59,in)  n
c
c Bit reverse algorithm for n bits
c
      Num = 2**(n-1) - 1
      do 10  I = 1, 2**(n-1)
        Num = Num + 1
c
c Reverse Num into B.
c The "and" function performs a bit-by-bit logical and
c to its arguments (Num and TwoToK in this case).
c
      B = 0.
      do 20  K = 0, N-1
        TwoToK = 2**K
        KthBit = and(Num,TwoToK)
        B = 2.*B + KthBit/TwoToK
20    continue
c
c B/(2**n) here is the I'th number in the bit reverse sequence
c
      write(59,9010)  B, B/(2**n)
c
10    continue
      call exit
c
9010  format ( f8.0, 4x, f15.8 )
      end
```

end

For n =	1, this produces	1 and bit reversed fraction plus $1/2N$ = 1/2
	2	1, 3 and 1/4, 3/4
	3	1, 5, 3, 7 and 1/8, 5/8, 3/8, 7/8
	4	1, 9, 5, 13, 3, 11, 7, 15 and 1/16 etc.
	5	1, 17, 9, 25, ... , 31 and 1/32 etc.

Both the Fibonacci and bit reversed methods tend to fill y_i space uniformly with only the first few x_i's (or with any partial set of the x_i's). This is the point of the uniformity seen in the figures. Hence, if v_i's are selected sequently [say, from inverting $f(v) \sim \exp -v^2/2v_t^2$], meaning highly ordered, then using these methods to scramble the x's will tend to produce the full $f(v)$ over a small region is x. This filling obviates the need for dividing x-space into sub regions each filled with $f(v)$ and then repeated.

Figure 3 shows (x,y) scatter plots where the y_i's are random numbers generated by the CRAY-1 computer and $x_i = (i - \frac{1}{2})/N$.

Figures 1, 2, and 3 appear to show that the Fibonacci number and bit reverse methods produces very good uniformity and that the random number generator produces considerable local (and probably global) bunching. Let us define a goodness number D, following *Wick* (1979) in order to measure the uniformity of the number sets just produced.

$$D \equiv \max\left|\frac{N_{xy}}{N} - xy\right| \tag{3}$$

for all x and y which satisfy

$$0 \leqslant x, y \leqslant 1 \tag{4}$$

and N_{xy} is the number of particles in the sub-rectangle (0,0), (0,y), (x,0), (x,y), *i.e.*,

$$0 \leqslant x_i \leqslant x \quad \text{and} \quad 0 \leqslant y_i \leqslant y \tag{5}$$

If the number set is uniformly distributed and N approaches infinity, the corresponding number D should be zero. D was calculated for the three methods mentioned above is shown in Figure 4 as a function of N. The Fibonacci number and bit reversed methods produce essentially the same degrees of uniformity with $D \approx 3/N$. The random number result is $D \approx 1/\sqrt{N}$. Hence, Fibonacci and bit reversed are smaller by roughly $3/\sqrt{N}$.

As a further test, we used the cumulative velocity distribution function to assign velocities v_x to a set of beams whose envelope is $f(v_x)$, and then used the three different number sets to scramble the particle positions, x. For a given Maxwellian velocity distribution function, the goodness of the local thermal equilibria were examined, by calculating the average of the first six velocity moments over a width $\Delta x < L$, the system length. We then compared the width Δx at which the average local velocity moments departed by 10% from the expected values, for each of the three different number sets. We found that for a large particle number $N(\gtrsim 10^3)$ both the Fibonacci number method and bit reversed method produce very good local thermal equilibria. Details will be given in the next QPR.

References

Neunzert, H., and J. Wick, The Convergence of Simulation Methods in Plasma Physics, *Proc. of Conf. on Math. Methods in Plasma Phys.*, Oberwolfach September 1979; published in *Methoden und Verfahren der mathematischen Physik*, P.Lang, Frankfurt, 1980.

Wick, J., Numerical Consequences of a Convergence Proof for PIC, *Proc. Ninth Conf. Num. Sim. Plasmas*, Northwestern Univ., Evanston, Ill., OB-2, June 1980.

Denavit, J., and J.M. Walsh, Time Filtering Particle Simulations with $\omega_{pe}\Delta t >> 1$, *Proc. Ninth Conf. Num. Sim. Plasmas*, Northwestern Univ., Evanston, Ill., PC-3, June 1980.

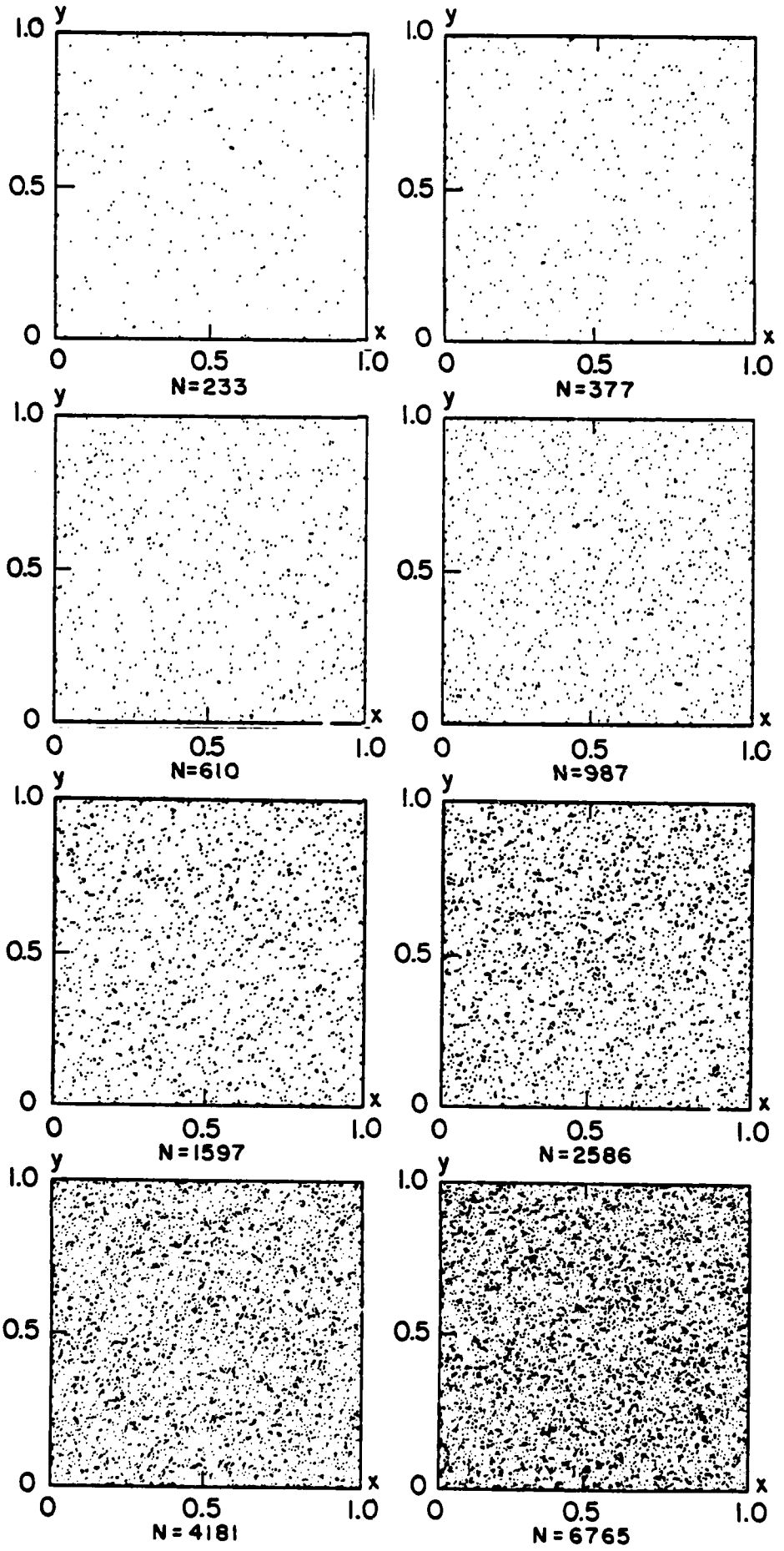

Figure 3. x,y_i space with the y_i chosen from then CRAY random number call.

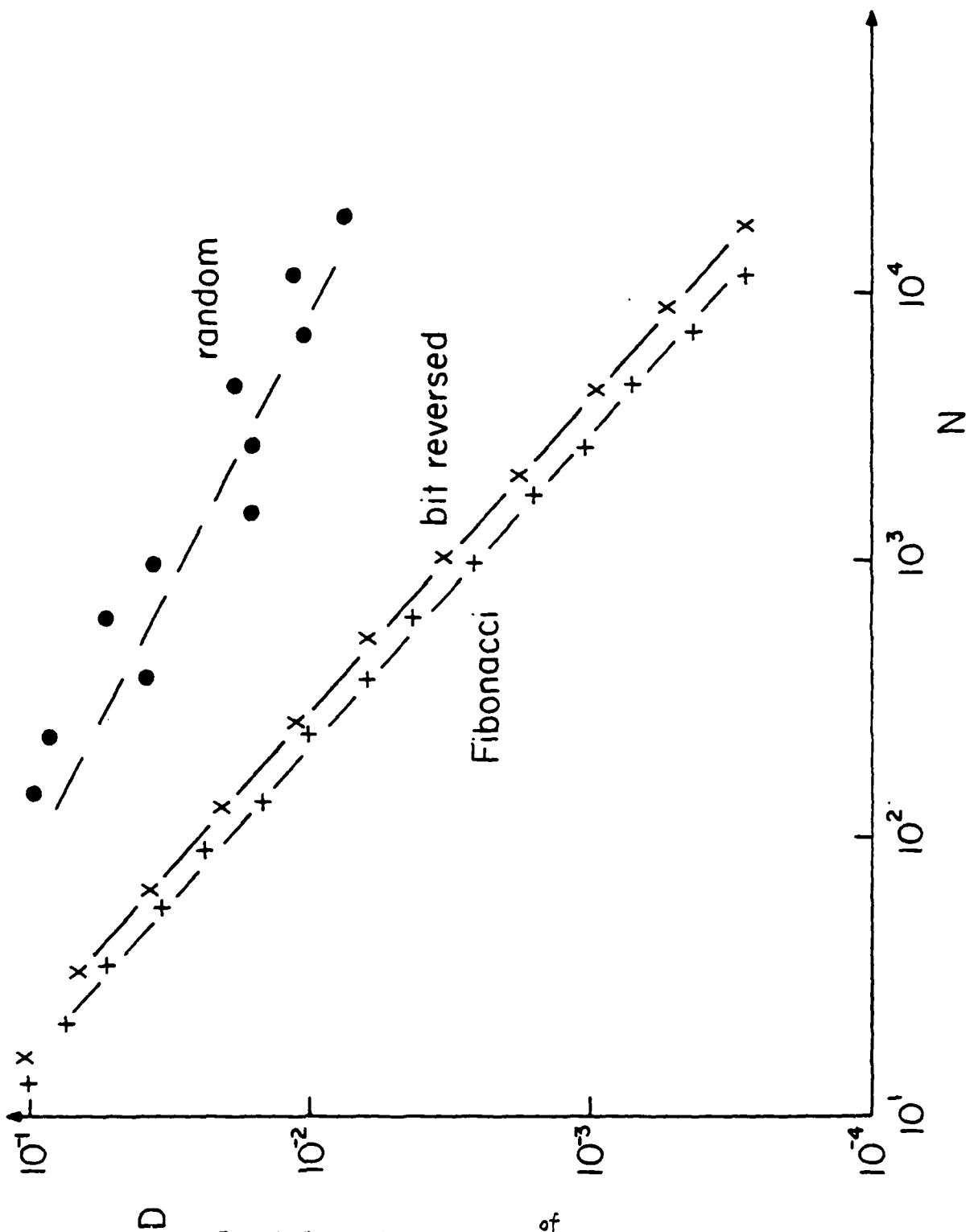

Figure 4. Goodness factor D as a function of N numbers, for random, Fibonacci and bit reversed methods. The dashed line in the random set is $D = 1/\sqrt{N}$. D for the Fibonacci and bit reversed numbers decay roughly as $3/N$.

F. *ESI Code*

No special progress to report.

G. *EMI Code*

No special progress to report.

H. *EZOHAR Code*

No special progress to report.

I. *RINGHYBRID Code*

No special progress to report.

SECTION III

SUMMARY OF REPORTS, TALKS, PUBLICATIONS, VISITORS

A. Talks

(a) Three talks were presented at the APS Division of Plasma Physics meeting Nov. 10 - 14, 1980, San Diego; the abstracts were given in the previous QPR.

(b) See paper by Harned in this QPR, presented at Compact Torus Meeting, Dec. 2 - 4, 1980, LASL.

B. Publications

ERL Memo. No. UCB/ERL M80/40 by Y-J Chen and C.K. Birdsall was accepted by Physics of Fluids.

ERL Memo No. UCB/ERL M80/20 by Y-J Chen and B.I. Cohen was accepted by Physics of Fluids.

C. Visitor

M.J. Gerver spent a week with us Nov. 1980.

D. Conference

Workshop on Long Time Steps in Particle Simulation, Dec. 8, 9, 1980 was organized by C.K. Birdsall and A. Friedman of UCB and B.I. Cohen and A.B. Langdon of LLL. The meeting notice and schedule follows:

WORKSHOP ON LONG TIME STEPS IN PARTICLE SIMULATION

December 8 and 9 (Monday and Tuesday), 1980
8:30 a.m. to 5:30 p.m.
Woodward Room
Bechtel Engineering Center
University of California, Berkeley

The recent work of Jacques Denavit and Rod Mason on implicit integration schemes and of Cohen et al., on orbit averaging has inspired this meeting. Many others have also contributed ideas on relaxing the numerical stability conditions on the time step in simulations.

The meeting format allows plenty of time for speakers and discussion. The tentative program is attached. The only special rule for the workshop is that one person speak at a time, as there is ample time for all viewpoints.

The objects of the workshop, in no special order, are:

to discuss in great detail Denavit and Mason's implicit schemes and the BAAL implicit algorithm

To collect ideas on $\omega_p \Delta >> 1$ stability and accuracy requirements and $kv\Delta t^p$ issues

appropriateness of centered vs. damping time integration algorithms

to address possible new problems associated with implicitness, e.g., generalizations to multidimensions and/or EM codes, boundary conditions, spatial filtering

to choose problem areas of importance for applications

to understand possible enhanced nosiness in implicit methods, e.g., due to collection of higher plasma moments

to design implicit time differencing algorithms

to consider melding implicit methods with time filtering and orbit-averaging methods in order to reduce noise

lastly, to categorize and generalize methods that do not and cannot work

* * * * * * * * *

The meeting room is a few steps from Cory Hall (northeast corner of Campus) where we have our computer terminals connected to NMFECC. Hence, we can try things out at any time during the workshop. This workshop is limited to the twenty people invited.

Charles K. Birdsall
Alex Friedman
EECS Dept., Cory Hall
University of California, Berkeley
Berkeley, CA 94720

Bruce Cohen
A. Bruce Langdon
Lawrence Livermore
National Laboratory

Schedule

Workshop on Long Time Steps in Particle Simulation, December 8, 9, 1980, U.C. Berkeley

Monday, 8:30 a.m. Welcoming remarks C.K. Birdsall

A. Morning Session 8:31 a.m. A. Bruce Langdon, Chairman		Time in Minutes
Jacques Denavit Northwestern	"Time Filtering Particle Simulations with $\omega_{pe}\Delta>>1$"	60
Rodney Mason LASL	"Implicit Moment Particle Simulation of Plasmas"	60
Jack Byers LLL	"Long Time Step Electrostatic Quasineutral Model for Magnetized Plasmas"	15
Vincent Thomas Bruce Cohen U.C. Berkeley	"Orbit Averaging in Implicit and Explicit Electrostatic Codes"	15

Lunch 12:30 Faculty Club, Lewis Room

B. Afternoon Session 1:30 p.m. Jack Byers, Chairman		
Jerry Brackbill David Forslund LASL	"Implicit Methods Applied to 2d, EM Codes"	60
A. Bruce Langdon Alex Friedman Bruce Cohen LLL	"BAAL Implicit Particle Algorithms"	60
Alex Friedman Bruce Cohen A. Bruce Langdon	"An Experimental BAAL Code"	60
Bruce Cohen A. Bruce Langdon Alex Friedman	"Design of Time Integration Algorithms"	60

Tuesday, 8:30 a.m.

C. Morning Session 8:30 a.m. Adam Drobot, Chairman

		Time in Minutes
W. W. Lee PPPL	"Gyrokinetic Particle Pushing Model" "Multiple Scale Simulation Model" (Simulation of drift wave problems in a homogenious plasma)	30
Brendan Godfrey MRC	"Iterative Inversion of Implicit Equations"	30
Viktor Decyk UCLA	"Dawson Long Time Step Schemes"	30
Bruce Cohen LLL	"Implicit Magneto-Inductive Hybrid Code, Orbit Averaging and Filtering"	
Robert Freis Bruce Cohen LLL	"2d Orbit Averaged Simulation of a Mirror Machine"	30

Lunch 12:30 Faculty Club, Lewis Room

D. Afternoon Session 1:30 p.m. C. K. Birdsall, Organizer

Rump Sessions, to be set up by discussion leaders picked during Sessions A,B,C, in order to cover topics needing more discussion.

End by 5:30 p.m.

Science Applications, Inc.

McBride, Siambis, Wagner

Sandia Laboratories, Albuquerque

Freeman, Poukey, Quintenz, Humphries

Sandia Laboratories, Livermore

Marx

Massachusetts

Johnston

Stanford University

Buneman

University of Arizona

Morse

University of California, Berkeley

Arons, Au Yeung, Birdsall, Chen, Chorin, Grisham, Harned, Hudson, Keith, Lichtenberg, Lieberman, McKee, Otani, Potter, Thomas

University of California, Davis

DeGroot, Woo

University of California, Irvine

Rynn

University of Calif., Los Angeles

Dawson, Decky, Huff, Lin

University of Iowa

Joyce, Knorr, Nicholson

University of Maryland

Guillory, Rowland, Winske

University of Pittsburgh

Zabusky

University of Texas

Horton, McMahon, Tajima

University of Wisconsin

Shohet

Culham Laboratory

Eastwood, Roberts

University of Reading

Hockney

Ecole Polytechnique/Centre de Physique Theoreque

Adam

Bhabha Atomic Research Centre

Aiyer, Gioel

Isreal

Gell

Tel-Aviv University

Cuperman

Kyoto University

Abe

Nagoya University

Kamimura

Max Planck Institut fur Plasmaphysik

Biskamp, Kraft

Universitat Kaiserslautern

Wick

DISTRIBUTION LIST

Department of Energy

Manley, Nelson, Sadowsky, Drobott
Lankford

Department of Navy

Condell, Roberson, Florance

Austin Research Associates

Drummond, Moore

Bell Telephone Laboratories

Hasegawa

Calif. Institute of Technology

Liewer

Calif. State Polytech. Univ.

Rathman

Columbia University

Chu

Cornell University

Mankofsky

Electrical Power Research Inst.

Gough, Scott

General Atomic Company

Helton, Lee

Hascom Air Force Base

Rulin

JAYCOR

Klein, Tumolillo, Hobbs

Kirtland Air Force Base

Pettus

Los Alamos Scientific Laboratory

Barnes, Forslund, Gitomer, Hewett, Lindemuth, Mason, Neilson, Oliphant, Sgro

Lawrence Berkeley Laboratory

Cooper, Kaufman, Kim, Kunkel, Pyle, Sternlieb

Lawrence Livermore National Laboratory

Albritton, Anderson, Brengle, Briggs, Bruijnes, Byers, Chambers, Cohen, Drupke, Estabrook, Fawley, Finan, Fries, Fuss, Harte, Killeen, Kruer, Langdon, Lasinski, Lee, Maron, Matsuda, Max, McNamara, Mirin, Nevins, Nielson, Smith, Tull, Friedman

Mass. Institute of Technology

Berman, Bers, Gerver, Kulp, Palevsky

Mission Research Corporation

Godfrey

U. S. Naval Research Laboratory

Boris, Drobot, Craig, Haber, Orens, Vomvoridis, Winsor

Northwestern University

Crystal, Denavit

New York University

Grad, Weitzner

Oak Ridge National Laboratory

Dory, Meier, Mook

Princeton Plasma Physics Laboratory

Chen, Cheng, Lee, Okuda, Tang

Princeton University

Graydon